

# Inertial Range Scaling, Kármán-Howarth Theorem and Intermittency for Forced and Decaying Lagrangian Averaged MHD in 2D

J. Pietarila Graham<sup>1</sup>, D. D. Holm<sup>2,3</sup>, P. Mininni<sup>1</sup> and A. Pouquet<sup>1</sup>

(Dated: Mar 1, 2006)

## Abstract

We present an extension of the Kármán-Howarth theorem to the Lagrangian averaged magnetohydrodynamic (*LAMHD*– $\alpha$ ) equations. The scaling laws resulting as a corollary of this theorem are studied in numerical simulations, as well as the scaling of the longitudinal structure function exponents indicative of intermittency. Numerical simulations for a magnetic Prandtl number equal to unity are presented both for freely decaying and for forced two dimensional MHD turbulence, solving directly the MHD equations, and employing the *LAMHD*– $\alpha$  equations at 1/2 and 1/4 resolution. Linear scaling of the third-order structure function with length is observed. The *LAMHD*– $\alpha$  equations also capture the anomalous scaling of the longitudinal structure function exponents up to order 8.

<sup>1</sup> National Center for Atmospheric Research, P.O. Box 3000, Boulder, CO 80307, USA

<sup>2</sup> Department of Mathematics, Imperial College London, London SW7 2AZ, UK

<sup>3</sup> Computer and Computational Science Division, Los Alamos National Laboratory, Los Alamos, NM 87545, USA

# 1 Introduction

Turbulent flows are ubiquitous in Nature and their very complexity make them hard to understand, let alone predict. One reason is that turbulence comes in intermittent “gusts”, such as fronts. These gusts are associated with their non-Gaussian statistics, which allows strong events occurring in the “fat tails” of the statistical distribution of, say, velocity gradients and other physical variables. From the theoretical viewpoint, its property of intermittency is the *sine qua non* of turbulence. Intermittency may also trigger large scale effects, such as the apparently random reversals of the Earth’s magnetic field [1]. It plays a role in other large scale events in the solar dynamo, and in the atmosphere of the earth. Although intermittency is believed to take place at small scales, strong events can affect the dynamics of the large scales, specially in systems close to criticality. For instance, Ref. [2] shows that local fluctuations of the kinetic helicity can explain phase and amplitude variations of the 22-years solar cycle. Intermittency is also one possible explanation for the occurrence of the Maunder-like minima of solar activity [3]. Finally, intermittency is known to affect the transport of momentum in atmospheric surface layers [4].

Intermittency is a highly spatially and temporally localized phenomenon, which thus requires high-resolution instrumentation, be it in the laboratory, in atmospheric and geophysical flows or in numerical simulations. In the latter case, the lack of adequate computer power (from the standpoint of the geo-physicist) implies that modeling of the unresolved small scales must take place. However, intermittency in general is not included explicitly in Large Eddy Simulations (LES) models of turbulent processes.

The intermittency of the subgrid-scale (SGS) energy dissipation as is usually defined in LES has been studied filtering 3D direct numerical simulations (DNS) of non-conductive fluids [5], with a Taylor Reynolds number  $R_\lambda = 150$ ; such a Reynolds number is somewhat insufficient for a determination of third-order scaling. For the SGS dissipation, they find that the Smagorinsky model, the volume-averaged dynamic model, and the similarity model perform fairly well (e.g. the error in the exponent for  $p = 7$  is less than 7%). On the other hand, the constant eddy-viscosity and spectral eddy-viscosity models underestimate intermittency beyond  $p = 4$  (compared to DNS) while the local and clipped dynamic Smagorinsky models strongly overestimate the intermittency beyond  $p = 4$ . In models not capturing intermittency properly, the question arises whether the overall statistics of the

flow at large scales would be affected by the absence of intermittency; and if so, how intermittency should be incorporated.

There are many models of turbulent flows (see for example the recent review in [6]) and there are many turbulent flows for which adequate testing of such models is in order. Magnetohydrodynamics, *i.e.* the coupling of a velocity and magnetic field at sub-luminal velocities so that the displacement current can be neglected, presents an interesting property, namely that in two space dimensions (2D), intermittency occurs as well as in three dimensions (3D). This is in contrast with the 2D neutral fluid case for which the conservation of vorticity leads to an inverse energy cascade to the large scales; in the presence of a magnetic field, this conservation is broken by the Lorentz force. Since, from a numerical standpoint, much higher Reynolds numbers can be achieved in 2D, an intermittent flow can be reached in 2D-MHD with adequate scale separation between the energy-containing range, the inertial range and the dissipation range. Our 2D MHD tests are able to exhibit a substantially larger Reynolds number (up to  $R_\lambda \sim 1500$ ) than the values listed for previous studies. This fact provides an ideal testing ground for models of turbulent MHD flows, such as they occur in geophysics and astrophysics: magnetic fields are observed in detail in the Earth and Sun environments, and are known to be dynamically important as well for the solar-terrestrial interactions (the so-called space weather), in the interstellar medium and in galaxies.

Modeling of MHD flows is still under development (see [7]). Most LES for hydrodynamic turbulence are based upon self-similarity or universality, in that they assume a known power law of the energy spectrum. For MHD, the kinetic energy is not a conserved quantity, and this poses a problem for the extension of such techniques to the case of MHD. Additional difficulties arise from the fact that MHD has several regimes depending on the relative strengths of the magnetic and velocity fields, their degree of alignment, and whether mechanical or magnetic energy is injected into the flow. However, some LES have been developed for particular cases. There exists LES for MHD turbulence with some degree of alignment between the velocity and magnetic fields [8], dissipative LES which does not model the interactions between the two fields [9], and LES for low magnetic Reynolds number [10]. We have recently tested one model which may be more generally applicable, the Lagrangian averaged magneto-hydrodynamics alpha (*LAMHD*- $\alpha$ ) model, both in 2D [11] and in 3D [12] and it has been used to examine the onset of the dynamo instability when the magnetic Prandtl number (the ra-

ratio of viscosity  $\nu$  to magnetic diffusivity  $\eta$ ) is small [13], as occurs in liquid metals in the laboratory, in the liquid core of the Earth or in the solar convection zone. In this context, because of the importance of intermittency as a fundamental, or even defining property of turbulence, we seek to determine to what extent *LAMHD*– $\alpha$  exhibits intermittency.

Intermittency is believed to be associated only with a forward cascade of energy; that is, the cascade of energy from larger scales to smaller scales, or, equivalently, from low wave numbers to high wave numbers. As previously mentioned, in determining the extent to which the *LAMHD*– $\alpha$  model exhibits intermittency, we shall take advantage of the forward cascade of energy which occurs in two-dimensional MHD. We shall first investigate the spectral scaling laws for this situation in Sec. 3, then its Kármán-Howarth theorem in Sec. 4. Section 4 also discusses the modifications of the Kármán-Howarth theorem for MHD which arise due to the presence of the length scale  $\alpha$  in the *LAMHD*– $\alpha$  model. The length scale  $\alpha$  modifies the nonlinearity in the motion equation, and one must estimate its observable physical effects. In particular, introduction of the length scale  $\alpha$  modifies the *LAMHD*– $\alpha$  energy spectrum for  $k\alpha > 1$ . Section 5 discusses energy conservation for the *LAMHD*– $\alpha$  model and investigates its inviscid energy dissipation anomaly, which arises from its scaling laws and its Kármán-Howarth theorem. Finally in Sec. 6 we investigate the effects of introducing the length scale  $\alpha$  on the intermittency of the *LAMHD*– $\alpha$  model solutions for decaying and forced turbulence in two dimensions. Just as for Navier-Stokes turbulence, these effects emerge in numerical simulations as a scaling anomaly in the higher order structure functions of the *LAMHD*– $\alpha$  model. Section 7 summarizes these results.

## 2 Background of the *LAMHD*– $\alpha$ model

### 2.1 The *LAMHD*– $\alpha$ model equations

The Lagrangian-averaged magnetohydrodynamic alpha, or *LAMHD*– $\alpha$  model was derived by Lagrangian averaging ordinary MHD along particle trajectories [14]. Specifically, the *LAMHD*– $\alpha$  equations arise from Lagrangian-averaging Hamilton’s principle for incompressible ideal MHD, after using a form of Taylor’s hypothesis of frozen-in turbulent fluctuations in the Euler-Poincaré equation for barotropic MHD from Ref. [15]. When Navier-Stokes

viscosity  $\nu$  and diffusivity  $\eta$  are included in the standard fashion, the equations for the *LAMHD*– $\alpha$  model emerge as,

$$\partial_t \mathbf{u} + \mathbf{u}_s \cdot \nabla \mathbf{u} - \mathbf{B}_s \cdot \nabla \mathbf{B} + (\nabla \mathbf{u}_s)^T \cdot \mathbf{u} + (\nabla \mathbf{B})^T \cdot \mathbf{B}_s + \nabla \pi = \nu \Delta \mathbf{u}, \quad (1)$$

$$\partial_t \mathbf{B}_s + \mathbf{u}_s \cdot \nabla \mathbf{B}_s - \mathbf{B}_s \cdot \nabla \mathbf{u}_s = \eta \Delta \mathbf{B}, \quad (2)$$

$$\operatorname{div} \mathbf{u}_s = 0, \quad \operatorname{div} \mathbf{B}_s = 0. \quad (3)$$

In these equations, subscript  $s$  denotes the smoothing obtained by inverting the Helmholtz relations,

$$\mathbf{u} = (1 - \alpha^2 \Delta) \mathbf{u}_s, \quad \mathbf{B} = (1 - \alpha_M^2 \Delta) \mathbf{B}_s. \quad (4)$$

with Dirichlet boundary conditions,

$$\mathbf{u}_s = 0 \quad \text{and} \quad \mathbf{B}_s = 0 \quad \text{on the boundary.}$$

The modified total pressure  $\pi$  in the motion equation for the *LAMHD*– $\alpha$  model is defined by

$$\pi + \frac{1}{2} |\mathbf{B}_s|^2 = p - \frac{1}{2} |\mathbf{u}_s|^2 - \frac{\alpha^2}{2} |\nabla \mathbf{u}_s|^2, \quad (5)$$

where  $p$  is the mechanical pressure. In these equations,  $\alpha$  and  $\alpha_M$  are two constant parameters:  $\alpha$  characterizes the correlation length between the instantaneous Lagrangian fluid trajectory and its mean (time average); while  $\alpha_M$  is its magnetic counterpart. These two parameters need not be equal, *ab initio*. The traditional MHD system is obtained by setting both  $\alpha = 0$  and  $\alpha_M = 0$ . Likewise, the *LANS*– $\alpha$  incompressible fluid turbulence model is obtained by setting  $\mathbf{B}_s = \mathbf{0}$ . These equations may also be obtained through a filtering approach, as proposed in the fluid case in [16].

## 2.2 Energy, momentum, circulation and linkages

The *LAMHD*– $\alpha$  system of equations (1-3) possesses the standard properties of a normal fluid theory. For example, the *LAMHD*– $\alpha$  system monotonically dissipates the positive energy

$$\mathcal{E} = \frac{1}{2} \int \left( \mathbf{u}_s \cdot \mathbf{u} + \mathbf{B}_s \cdot \mathbf{B} \right) d^3x, \quad (6)$$

according to

$$\frac{d\mathcal{E}}{dt} = -\nu \int \left( |\nabla \mathbf{u}_s|^2 + \alpha^2 |\Delta \mathbf{u}_s|^2 \right) d^3x - \eta \int \left( |\nabla \mathbf{B}|^2 + \alpha^2 |\Delta \mathbf{B}|^2 \right) d^3x. \quad (7)$$

In addition, the *LAMHD*– $\alpha$  motion equation (1) may be expressed in conservative form as

$$\frac{\partial}{\partial t} u_i = - \frac{\partial}{\partial x^j} \left( T_i^j - \nu u_{i,l} \delta^{lj} \right), \quad (8)$$

with stress tensor

$$\begin{aligned} T_i^j &= \left( u_i u_s^j - \alpha^2 u_{s k, i} u_s^{k, j} \right) - \left( B_i B_s^j - \alpha^2 B_{s k, i} B_s^{k, j} \right) \\ &+ \delta_i^j \left( p - \frac{1}{2} |\mathbf{B}_s|^2 + \mathbf{B}_s \cdot \mathbf{B} - \frac{\alpha^2}{2} |\nabla \mathbf{B}_s|^2 \right). \end{aligned} \quad (9)$$

Thus, the two velocities appearing in the *LAMHD*– $\alpha$  model may be interpreted as fluid parcel velocity  $\mathbf{u}_s$  and momentum per unit mass  $\mathbf{u}$ .

The Kelvin circulation theorem for the incompressible *LAMHD*– $\alpha$  motion equation (1) involves both of these velocities,

$$\frac{d}{dt} \oint_{c(\mathbf{u}_s)} \mathbf{u} \cdot d\mathbf{x} = \oint_{c(\mathbf{u}_s)} (\mathbf{J} \times \mathbf{B}_s + \nu \Delta \mathbf{u}) \cdot d\mathbf{x}, \quad (10)$$

where  $\mathbf{J} = \text{curl } \mathbf{B}$ . Hence, the  $\mathbf{J} \times \mathbf{B}_s$  force and viscous force can each generate circulation of  $\mathbf{u}$  around material loops moving with smoothed velocity  $\mathbf{u}_s$ . This results by Stokes theorem in vorticity dynamics for  $\boldsymbol{\omega} = \text{curl } \mathbf{u}$  in the form

$$\frac{\partial \boldsymbol{\omega}}{\partial t} + \mathbf{u}_s \cdot \nabla \boldsymbol{\omega} - \boldsymbol{\omega} \cdot \nabla \mathbf{u}_s = \mathbf{B}_s \cdot \nabla \mathbf{J} - \mathbf{J} \cdot \nabla \mathbf{B}_s + \nu \Delta \boldsymbol{\omega}. \quad (11)$$

The linkages of the smooth B-field  $\mathbf{B}_s$  with itself and with the vorticity  $\boldsymbol{\omega}$  are given respectively by the helicity  $\int \mathbf{A}_s \cdot \mathbf{B}_s d^3x$  and cross helicity  $\int \mathbf{u} \cdot \mathbf{B}_s d^3x$ . The densities for these linkages satisfy

$$\frac{\partial}{\partial t} (\mathbf{A}_s \cdot \mathbf{B}_s) + \text{div} \left( (\mathbf{A}_s \cdot \mathbf{B}_s) \mathbf{u}_s \right) = \eta (\mathbf{A} \cdot \mathbf{B}_s + \mathbf{A}_s \cdot \mathbf{B}), \quad (12)$$

in which  $\mathbf{B}_s = \text{curl } \mathbf{A}_s$  and  $\mathbf{B} = \text{curl } \mathbf{A}$ , and, cf. (5),

$$\frac{\partial}{\partial t} (\mathbf{u} \cdot \mathbf{B}_s) + \text{div} \left( (\mathbf{u} \cdot \mathbf{B}_s) \mathbf{u}_s + \left( \pi + \frac{1}{2} |\mathbf{B}_s|^2 \right) \mathbf{B}_s \right) = \nu \mathbf{B}_s \cdot \Delta \mathbf{u} + \eta \mathbf{u} \cdot \Delta \mathbf{B}. \quad (13)$$

Thus, resistivity affects the helicity, while both resistivity and viscosity affect the cross helicity, and these linkages are both preserved by *LAMHD*– $\alpha$  in the ideal case. Of course, these properties of energy, momentum, circulation and linkages for the *LAMHD*– $\alpha$  model all reduce to characteristics of normal MHD, when  $\alpha^2 \rightarrow 0$ .

### 2.3 Recasting *LAMHD*– $\alpha$ as an LES turbulence model

The *LAMHD*– $\alpha$  model modifies the motion equation for ordinary MHD. By a short sequence of manipulations, we may recast the *LAMHD*– $\alpha$  motion equation into a form which is reminiscent of an LES turbulence model. We begin with the following commutation relation,

$$[\mathbf{p} \cdot \nabla, (1 - \alpha^2 \Delta)] \mathbf{q} = \alpha^2 \operatorname{div} (\nabla \mathbf{q} \cdot \nabla \mathbf{p} + \nabla \mathbf{q} \cdot \nabla \mathbf{p}^T) - \alpha^2 (\nabla(\operatorname{div} \mathbf{p}) \cdot \nabla) \mathbf{q} \quad (14)$$

which holds for any vectors  $\mathbf{p}$  and  $\mathbf{q}$ . Two other useful vector identities are,

$$(\nabla \mathbf{u}_s)^T \cdot \mathbf{u} - \nabla \left( \frac{1}{2} |\mathbf{u}_s|^2 + \frac{\alpha^2}{2} |\nabla \mathbf{u}_s|^2 \right) = -\alpha^2 \operatorname{div} (\nabla \mathbf{u}_s^T \cdot \nabla \mathbf{u}_s), \quad (15)$$

$$(\nabla \mathbf{B})^T \cdot \mathbf{B}_s - \nabla \left( \frac{1}{2} (1 - \alpha^2 \Delta) |\mathbf{B}_s|^2 + \frac{\alpha^2}{2} |\nabla \mathbf{B}_s|^2 \right) = \alpha^2 \operatorname{div} (\nabla \mathbf{B}_s^T \cdot \nabla \mathbf{B}_s) \quad (16)$$

where  $\alpha = \alpha_M$  was assumed. Consequently, the motion equation in the incompressible *LAMHD*– $\alpha$  model may be rewritten equivalently in “LES form” as,

$$(1 - \alpha^2 \Delta) (\partial_t \mathbf{u}_s + \mathbf{u}_s \cdot \nabla \mathbf{u}_s - \mathbf{B}_s \cdot \nabla \mathbf{B}_s + \nabla p_s - \nu \Delta \mathbf{u}_s) = -\alpha^2 \operatorname{div} \tau, \quad (17)$$

where the divergence of the “stress tensor”  $\tau$  is given by

$$\begin{aligned} \operatorname{div} \tau = & \operatorname{div} (\nabla \mathbf{u}_s \cdot \nabla \mathbf{u}_s + \nabla \mathbf{u}_s \cdot \nabla \mathbf{u}_s^T - \nabla \mathbf{u}_s^T \cdot \nabla \mathbf{u}_s) \\ & - \operatorname{div} (\nabla \mathbf{B}_s \cdot \nabla \mathbf{B}_s + \nabla \mathbf{B}_s \cdot \nabla \mathbf{B}_s^T - \nabla \mathbf{B}_s^T \cdot \nabla \mathbf{B}_s), \end{aligned} \quad (18)$$

and gradient terms have been absorbed into the modified total pressure, denoted by  $\tilde{\pi}$ , which is given by

$$\tilde{\pi} = p - \frac{1}{2} |\mathbf{u}_s|^2 - \frac{\alpha^2}{2} |\nabla \mathbf{u}_s|^2 - \frac{1}{2} (1 - \alpha^2 \Delta) |\mathbf{B}_s|^2 - \frac{\alpha^2}{2} |\nabla \mathbf{B}_s|^2, \quad (19)$$

where  $p = (1 - \alpha^2 \Delta)p_s$ . By using the following identity for divergenceless vectors  $\text{div } \mathbf{u} = 0$

$$\text{div} (\nabla \mathbf{u}^T \cdot \nabla \mathbf{u}^T) = \nabla \frac{1}{2} \text{tr} (\nabla \mathbf{u} \cdot \nabla \mathbf{u}), \quad (20)$$

we may rewrite the added stress in (18) equivalently, as

$$\text{div } \tau = 4 \text{div} (S \cdot \Omega - \Sigma \cdot J) + \nabla \Pi \quad (21)$$

with new notation

$$\begin{aligned} S &= \frac{1}{2} (\nabla \mathbf{u}_s + \nabla \mathbf{u}_s^T), & \Omega &= \frac{1}{2} (\nabla \mathbf{u}_s - \nabla \mathbf{u}_s^T) \\ \Sigma &= \frac{1}{2} (\nabla \mathbf{B}_s + \nabla \mathbf{B}_s^T), & J &= \frac{1}{2} (\nabla \mathbf{B}_s - \nabla \mathbf{B}_s^T), \end{aligned}$$

and additional pressure

$$\Pi = \frac{1}{2} \text{tr} (\nabla \mathbf{u}_s \cdot \nabla \mathbf{u}_s) - \frac{1}{2} \text{tr} (\nabla \mathbf{B}_s \cdot \nabla \mathbf{B}_s).$$

The (non-symmetric) stress tensor  $\tau$  given by

$$\tau = 4 (S \cdot \Omega - \Sigma \cdot J) + \text{Id } \Pi \quad (22)$$

which emerges from these manipulations casts the *LAMHD*– $\alpha$  model into a form reminiscent of an LES turbulence model. We shall find these expressions convenient below in introducing the analog of Elsässer variables for the *LAMHD*– $\alpha$  model.

### 3 Inertial range scaling laws in forward energy cascade

In two space dimensions, the conservation of vorticity in the neutral ( $\mathbf{B} \equiv 0$  case) leads to an inverse energy cascade; however, the Lorentz force breaks this conservation and, in MHD, energy is found to be mostly transferred to the small scales both in 2D and in 3D. Several measurements, starting with satellite data in the solar wind and continuing more recently with direct numerical simulations both in two dimensions and three dimensions, indicate



that the energy spectrum of a turbulent MHD flow follows a law that is barely distinguishable from a neutral fluid, with  $E(k) \sim k^{-1.70}$ . Differences do occur when one examines higher order structure functions: the most intermittent case (almost comparable in magnitude to that of the passive scalar) is the two-dimensional MHD fluid; three-dimensional MHD appears less intermittent than the 2D MHD case [17], and the 3D neutral fluid is the lesser intermittent of the three. Intermittency has been observed in the Solar Wind as well. None of the data at the second order level is in agreement with the phenomenologies developed by Kolmogorov [18] and leading to an energy spectrum  $E(k) \sim k^{-5/3}$  (heretofore the K41 model) or by Iroshnikov and by Kraichnan [19] (heretofore, the IK model) and leading to a shallower spectrum, *viz.*  $E(K) \sim k^{-3/2}$  in the absence of significant velocity-magnetic field correlations. These two types of phenomenology differ by the taking into account in the latter case of the non-local interactions (in Fourier space) emanating from the propagation of Alfvén waves; it is worth mentioning here that the IK model also agrees with the isotropic limit of the weak turbulence theory for incompressible MHD [20]. Note also that a model of intermittency for MHD flows [21] does recover the intermittency as measured in direct numerical simulations both in 2D [21] and in 3D [17], but such models depend on two adjustable parameters and thus do not necessarily have a predictive power.

These anomalous scaling laws are not fully understood but, for the neutral case, there is an exact law at third order with which the K41 phenomenology is compatible. In MHD, the exact law is more complex in its structure since it involves third-order cross-correlations between the velocity and the magnetic field [22] whereas the phenomenologies evoked above refer to single-variable moments. In that instance, it is worth asking what is the equivalent exact law in the context of the *LAMHD*– $\alpha$  model, a task developed in the next section. The question also arises as to what is the spectrum of energy beyond the alpha cut-off scales (which we take equal here, although different choices can be made, see *e.g.* [12, 13]). The answer should be guided by what is the pseudo-invariant in the small scales, beyond  $\alpha$ . In the neutral fluid case, it is the enstrophy  $\langle \omega^2 \rangle$  and in MHD this becomes  $\langle \omega^2 \rangle + \langle j^2 \rangle$ , where  $\mathbf{j}$  is the current density. A Kolmogorov-like dimensional reasoning (see [23] for the *LANS*– $\alpha$  case) taking into account this pseudo-invariance law will lead to a  $k^{-3}$  spectrum at scales smaller than  $\alpha$  whereas it can be easily shown that the corresponding IK arguments lead to a  $k^{-5/2}$  law.

## 4 Kármán-Howarth theorem for $LAMHD-\alpha$ in 2D and 3D Elsässer variables

In 1938, Kármán and Howarth [24] introduced the invariant theory of isotropic hydrodynamic turbulence, and derived from the Navier-Stokes equations an exact law relating the time derivative of the two-point velocity correlation with the divergence of the third-order correlation function. Later, this result was generalized to the MHD case by Chandrasekar [25], and recently written in terms of Elsässer variables [22]. For  $LANS-\alpha$  in the fluid case it was derived in [26]. The relevance of the Kármán-Howarth theorem for the study of turbulence cannot be underestimated. As a corollary, rigorous scaling laws in the inertial range can be deduced. In this section we will generalize these results to the  $LAMHD-\alpha$  case.

For the sake of simplicity, we will consider the case  $\eta = \nu = 0$ , the dissipative terms can be added at any point in the derivation. Also, we will use  $\alpha = \alpha_M$ . We start writing the  $LAMHD-\alpha$  equations using the Elsässer variables

$$\mathbf{z}^\pm = \mathbf{u} \pm \mathbf{B}, \quad \mathbf{z}_s^\pm = \mathbf{u}_s \pm \mathbf{B}_s. \quad (23)$$

Applying the Helmholtz operator to eq. (2), we obtain

$$(1 - \alpha^2 \Delta) (\partial_t \mathbf{B}_s + \mathbf{u}_s \cdot \nabla \mathbf{B}_s - \mathbf{B}_s \cdot \nabla \mathbf{u}_s) = 0. \quad (24)$$

Now we add and subtract eqs. (17) and (24). Using eqs. (23) we obtain equations for the evolution of  $\mathbf{z}_s^\pm$ ,

$$(1 - \alpha^2 \Delta) (\partial_t \mathbf{z}_s^\pm + \mathbf{z}_s^\mp \cdot \nabla \mathbf{z}_s^\pm + \nabla \tilde{\pi}_s) = -\alpha^2 \text{div } \tau, \quad (25)$$

where the stress tensor divergence  $\text{div } \tau$  in terms of the Elsässer variables is

$$\begin{aligned} \text{div } \tau = & \frac{1}{2} \text{div} \left( \nabla \mathbf{z}_s^+ \cdot \nabla \mathbf{z}_s^- + \nabla \mathbf{z}_s^+ \cdot \nabla \mathbf{z}_s^{-T} - \nabla \mathbf{z}_s^{+T} \cdot \nabla \mathbf{z}_s^- \right. \\ & \left. + \nabla \mathbf{z}_s^- \cdot \nabla \mathbf{z}_s^+ + \nabla \mathbf{z}_s^- \cdot \nabla \mathbf{z}_s^{+T} - \nabla \mathbf{z}_s^{-T} \cdot \nabla \mathbf{z}_s^+ \right). \end{aligned} \quad (26)$$

This stress divergence may be rewritten equivalently, as

$$\begin{aligned} \operatorname{div} \tau &= 2 \operatorname{div} \left( \Delta^+ \cdot \Sigma^- + \Delta^- \cdot \Sigma^+ \right) + \nabla \Pi \\ \text{with } \Sigma^\pm &= \frac{1}{2} \left( \nabla \mathbf{z}^\pm + (\nabla \mathbf{z}^\pm)^T \right), \quad \Delta^\pm = \frac{1}{2} \left( \nabla \mathbf{z}^\pm - (\nabla \mathbf{z}^\pm)^T \right), \end{aligned}$$

with the same additional pressure  $\Pi$  as before.

We could repeat all the derivation to obtain an equation for the evolution of  $\mathbf{z}^\pm$  from eqs. (1) and (24). Instead, starting from eq. (25), using eqs. (4) and (14) we obtain

$$\partial_t \mathbf{z}^\pm + \mathbf{z}_s^\mp \cdot \nabla \mathbf{z}^\pm + \nabla \tilde{\pi} = \alpha^2 \operatorname{div} \zeta^\pm \quad (27)$$

where

$$\begin{aligned} \zeta^\pm &= \frac{1}{2} \left( \nabla \mathbf{z}_s^\pm \cdot \nabla \mathbf{z}_s^\mp + \nabla \mathbf{z}_s^\pm \cdot \nabla \mathbf{z}_s^\mp{}^T + \nabla \mathbf{z}_s^{\pm T} \cdot \nabla \mathbf{z}_s^\mp \right. \\ &\quad \left. - \nabla \mathbf{z}_s^\mp \cdot \nabla \mathbf{z}_s^\pm - \nabla \mathbf{z}_s^\mp \cdot \nabla \mathbf{z}_s^{\pm T} + \nabla \mathbf{z}_s^{\mp T} \cdot \nabla \mathbf{z}_s^\pm \right). \end{aligned} \quad (28)$$

Note that equations (25) and (27) make explicit the fact that Alfvén waves  $\mathbf{u} = \pm \mathbf{B}$ ,  $\mathbf{u}_s = \pm \mathbf{B}_s$  are exact nonlinear solutions of the *LAMHD*– $\alpha$  equations. For an Alfvén wave either  $\mathbf{z}^+$  or  $\mathbf{z}^-$  (as well as the corresponding field  $\mathbf{z}_s^\pm$ ) is zero. In this case, all nonlinear terms are zero and verification of the solution follows.

In Cartesian coordinates, we can write equations (25) and (27) in components

$$\partial_t z_i^\pm + \partial_k \left( z_i^\pm z_s^{\mp k} + \tilde{\pi} \delta_i^k - \alpha^2 \zeta_i^{\pm k} \right) = 0 \quad (29)$$

$$\partial_t z'_s j^\pm + \partial'_k \left( z'_j{}^\pm z'_s{}^{\mp k} + \tilde{\pi}'_s \delta_j^k + \alpha^2 g_\alpha * \tau'^k_j \right) = 0, \quad (30)$$

the prime denotes that the variables are evaluated at  $\mathbf{x}'$ , and

$$g_\alpha = \frac{e^{-r/\alpha}}{4\pi\alpha^2 r} \quad (31)$$

is the Yukawa potential. The Green function of the Helmholtz operator is

given by

$$g_\alpha * \tau_i^k = \int g_\alpha (|\mathbf{x}' - \mathbf{x}|) \tau_i^k(\mathbf{x}') d^3 x', \quad (32)$$

and the components of the stress tensors  $\tau$  and  $\zeta^\pm$  are

$$\begin{aligned} \tau_i^k &= \frac{1}{2} \left( \partial_j z_{s_i}^+ \partial^k z_s^{-j} + \partial_j z_{s_i}^+ \partial^j z_s^{-k} - \partial_i z_{s_j}^+ \partial^k z_s^{-j} \right. \\ &\quad \left. + \partial_j z_{s_i}^- \partial^k z_s^{+j} + \partial_j z_{s_i}^- \partial^j z_s^{+k} - \partial_i z_{s_j}^- \partial^k z_s^{+j} \right), \end{aligned} \quad (33)$$

$$\begin{aligned} \zeta_i^{\pm k} &= \frac{1}{2} \left( \partial_j z_{s_i}^\pm \partial^k z_s^{\mp j} + \partial_j z_{s_i}^\pm \partial^j z_s^{\mp k} + \partial_i z_{s_j}^\pm \partial^k z_s^{\mp j} \right. \\ &\quad \left. - \partial_j z_{s_i}^\mp \partial^k z_s^{\pm j} - \partial_j z_{s_i}^\mp \partial^j z_s^{\pm k} + \partial_i z_{s_j}^\mp \partial^k z_s^{\pm j} \right). \end{aligned} \quad (34)$$

Multiplying eq. (29) by  $z'_{s_j}^\pm$ , eq. (30) by  $z_i^\pm$ , and adding the result yields

$$\begin{aligned} \partial_t \langle z_i^\pm z'_{s_j}^\pm \rangle &= \frac{\partial}{\partial r^k} \langle (z_i^\pm z_s^{\mp k} - \alpha^2 \zeta_i^{\pm k}) z'_{s_j}^\pm \rangle + \frac{\partial}{\partial r^k} \langle \tilde{\pi}' z'_{s_j}^\pm \delta_i^k - \tilde{\pi}'_s z_i^\pm \delta_j^k \rangle \\ &\quad - \frac{\partial}{\partial r^k} \langle (z'_{s_j}^\pm z_s^{\pm k} + \alpha^2 g_\alpha * \tau_j^k) z_i^\pm \rangle, \end{aligned} \quad (35)$$

where we used homogeneity

$$\frac{\partial}{\partial r^k} \langle \cdot \rangle = \frac{\partial}{\partial x'^k} \langle \cdot \rangle = -\frac{\partial}{\partial x^k} \langle \cdot \rangle. \quad (36)$$

Now, we can make the equation symmetric in the indices  $i, j$  adding the equation for  $\partial_t \langle z_j^\pm z'_{s_i}^\mp \rangle$ . We use homogeneity

$$\langle q_i q'_{s_j} q_s^k + q_j q'_{s_i} q_s^k \rangle = -\langle q'_i q_{s_j} q_s^k + q'_j q_{s_i} q_s^k \rangle, \quad (37)$$

and define the tensors

$$\mathcal{Q}_{ij}^\pm = \langle z_i^\pm z'_{s_j}^\pm + z_j^\pm z'_{s_i}^\pm \rangle, \quad (38)$$

$$\mathcal{T}^{\pm k}_{ij} = \langle (z_i^\pm z'_{s_j}^\pm + z_j^\pm z'_{s_i}^\pm + z_i^\pm z_{s_j}^\pm + z_j^\pm z_{s_i}^\pm) z_s^{\mp k} \rangle, \quad (39)$$

$$\mathcal{I}^{\pm k}_{ij} = \langle (\tilde{\pi}'_s z_j^\pm - \tilde{\pi}' z'_{s_j}^\pm) \delta_i^k + (\tilde{\pi}'_s z_i^\pm - \tilde{\pi}' z'_{s_i}^\pm) \delta_j^k \rangle, \quad (40)$$

$$\mathcal{S}^{\pm k}_{ij} = \langle \tau_i^k z'_{s_j}^\pm + \tau_j^k z'_{s_i}^\pm + g_\alpha * \tau'_{s_j}{}^k z_i^\pm + g_\alpha * \tau'_{s_i}{}^k z_j^\pm \rangle. \quad (41)$$

We can drop  $\Pi^{\pm k}_{ij}$  because the terms with the pressures  $\tilde{\pi}$  and  $\tilde{\pi}'_s$  vanish everywhere, as follows from the usual arguments of isotropy [24]. Finally we obtain

$$\partial_t \mathcal{Q}_{ij}^{\pm} = \frac{\partial}{\partial r^k} \left( \mathcal{T}^{\pm k}_{ij} - \alpha^2 \mathcal{S}^{\pm k}_{ij} \right). \quad (42)$$

This is the *LAMHD*– $\alpha$  version of eq. (3.8) in [26]. In the case  $\alpha = 0$  this equation is also a linear combination of eq. (43), (50), and (56) in [25]. More Kármán-Howarth equations can be written for different combinations of  $z^{\pm}$  and  $z_s^{\mp}$ .

Since  $\mathcal{Q}_{ij}^{\pm}$  and  $\mathcal{T}^{\pm k}_{ij}$  are symmetric and divergence free in their indices  $i$  and  $j$ ,  $\mathcal{S}^{\pm k}_{ij}$  must be symmetric and divergence free in  $i$  and  $j$ . But the Elsässer variables  $\mathbf{z}^{\pm}$  are combinations of vectors and pseudovectors. Therefore,  $\mathcal{Q}^{\pm}$  is a combination of tensors and pseudotensors. We can define a tensor as

$$\mathcal{Q} = \mathcal{Q}^{\pm} + \mathcal{Q}^{\mp}, \quad (43)$$

and a pseudotensor as  $\mathcal{Q}^{\pm} - \mathcal{Q}^{\mp}$ . We will continue using only the tensor  $\mathcal{Q}$ , the results can also be obtained for the pseudotensors using the expressions in [25]. We also define  $\mathcal{T} = \mathcal{T}^{\pm} + \mathcal{T}^{\mp}$  and  $\mathcal{S} = \mathcal{S}^{\pm} + \mathcal{S}^{\mp}$ .

Imposing isotropy and from incompressibility,  $\mathcal{Q}$  can be written as [27]

$$\mathcal{Q}_{ij} = \text{curl}(Q r_l \epsilon_{ijl}) = -(d+1)Q \delta_{ij} + r Q' \left( \frac{r_i r_j}{r} - \delta_{ij} \right), \quad (44)$$

where the curl is taken with respect to the third index ( $j$ ),  $Q = Q(r, t)$  is a scalar function,  $\epsilon$  is the Levi-Civita pseudotensor, and  $d$  is the number of dimensions. Here,  $Q' = \partial_r Q$ .

In the same way, we can write

$$\begin{aligned} \mathcal{T}_{ij}^k &= \text{curl} [T (r_i \epsilon_{jkl} r^l + r_j \epsilon_{ikl} r^l)] \\ &= \frac{2}{r} T' r_i r_j r^k - (r T' + d T) (r_i \delta_j^k + r_j \delta_i^k) + 2 T \delta_{ij} r^k. \end{aligned} \quad (45)$$

The tensor  $\mathcal{S}$  takes the same form with scalar function  $S(r, t)$ . Note that  $\mathcal{S}$  is the isotropic sub- $\alpha$ -scale stress tensor in the LES formulation of *LAMHD*– $\alpha$ .

Now we compute the divergence of these tensors. In three dimensions

$$\frac{\partial}{\partial r^k} \mathcal{T}_{ij}^k = \text{curl} [(r T' + 5 T) \epsilon_{ijl} r^l], \quad (46)$$

and the divergence for  $\mathcal{S}$  takes the same form. Replacing eqs. (44) and (46) into eq. (42) we finally obtain

**Theorem 1 (Karman-Howarth Theorem for LAMHD- $\alpha$ )**

*The exact LAMHD- $\alpha$  model relation (42) for homogeneous isotropic statistics implies the isotropic tensor relation in three dimensions*

$$\frac{\partial Q}{\partial t} = \left( r \frac{\partial}{\partial r} + 5 \right) (T^2 - \alpha^2 S), \quad (47)$$

and in  $d$  dimensions the general result is

$$\frac{\partial Q}{\partial t} = \left[ r \frac{\partial}{\partial r} + (d + 2) \right] (T^2 - \alpha^2 S). \quad (48)$$

This is the generalization of the Kármán-Howarth equation for LAMHD- $\alpha$  (two more equations can be written for different combinations of the tensors and pseudotensors), without the dissipation. When  $\mathbf{B} = 0$  this equation is also eq. (3.16) in [26]. When  $\alpha = 0$ , this is equivalent to the Kármán-Howarth equation for the Elsässer variables as derived in [22], or a combination of equations (49) and (53) in [25].

Therefore, all equations in [22] follow for  $\alpha/r \ll 1$ . This result confirms that the alpha-model preserves the properties of MHD for separations larger than  $r \sim \alpha$ . For  $r > \alpha$ , the scaling of structure functions and the relation between second and third order functions hold.

**Corollary 2 (Kolmogorov Theorem for LAMHD- $\alpha$ )**

*Introducing the flux  $\partial_t Q = -2\epsilon_\alpha/d$  with  $\epsilon_\alpha = \epsilon_\alpha^+ + \epsilon_\alpha^-$  (the energy injection rate for each Elsässer variable) in eq. (48) and integrating in the inertial range yields*

$$- \frac{2}{d(d+2)} \epsilon_\alpha = (T - \alpha^2 S), \quad (49)$$

where  $T$  and  $S$  are defined in equations (39) and (41).

Note a multiplicative factor compared with the usual expression from Kolmogorov, related to the relation between autocorrelation functions and structure functions in isotropic turbulence in  $d$  dimensions. For  $\alpha/r \ll 1$  this equation reduces again to the MHD results. Note also that structure and autocorrelation functions in LAMHD- $\alpha$  involve one unsmoothed field and

one smoothed field if quantities are of second order, and two smoothed fields if quantities are of third order. In the following sections, we will use this convention and all structure functions for *LAMHD*– $\alpha$  will be written as they follow from the expressions of the tensors  $\mathcal{Q}$  and  $\mathcal{T}$ .

## 5 Energy dissipation anomaly

The Kármán–Howarth (KH) theorem for fluid turbulence [24] gives the exact analytical relation between the time rate of change of the second-order two-point velocity correlation function and the gradient of the third-order two-point velocity correlation function, as derived from the Navier-Stokes equation for homogeneous, isotropic turbulence.

Kolmogorov [18] used the structure function form of the KH equation, to show – for homogeneous, isotropic and stationary turbulence, in the limit  $\nu \rightarrow 0$  of vanishing kinematic viscosity – that the Navier-Stokes equations lead to an exact relationship between the third-order structure function and the energy dissipation rate,  $\bar{\epsilon}$ , which scales linearly in the separation,  $r$ . This is Kolmogorov’s famous “four-fifths law.”

By assuming self-similarity of scales in the inertial range Kolmogorov then was able to deduce, in steps that essentially amount to dimensional analysis, that the second-order structure function must scale as  $r^{2/3}$  and that consequently the energy spectrum (which is essentially the Fourier transform of the second-order structure function) must scale as  $k^{-5/3}$ . As noted in [28], Kolmogorov’s four-fifths law

is one of the most important results in fully developed turbulence because it is both exact and nontrivial. It thus constitutes a kind of ‘boundary condition’ on theories of turbulence: such theories, to be acceptable, must either satisfy the four-fifths law, or explicitly violate the assumptions made in deriving it.

The two key assumptions in Kolmogorov’s derivation of the four-fifths law are that (1) an inertial range exists in which the flow is self-similar and (2) the energy dissipation rate does not change as one takes the limit  $\nu \rightarrow 0$ .

The equivalent of the KH equation was derived for the *LANS*– $\alpha$  model in [26]. Since the model relates the Helmholtz smoothed velocity  $\mathbf{u}_s$ , to the unsmoothed velocity  $\mathbf{u}$ , the appropriate correlation functions that emerge are the second- and third-order two-point correlation between  $\mathbf{u}_s$  and  $\mathbf{u}$ .

Upon following Kolmogorov’s analysis for isotropic inertial range statistics, the corollary to the  $LANS-\alpha$  KH-equation is that solutions of the  $LANS-\alpha$  equations possess two regimes of scaling, depending on whether the separation distance  $r$  is greater, or less than the size  $\alpha$ . For  $r > \alpha$ , the third-order correlation scales like  $r$ , thereby recovering Navier-Stokes behavior. In contrast, for  $r < \alpha$  the third-order correlation scales like  $r^3$ . If self-similarity is then assumed one finds for  $r > \alpha$  that the second-order correlation scales like  $r^{2/3}$ , again recovering Navier-Stokes behavior. However, for  $r < \alpha$  the second-order correlation scales like  $r^2$ . Correspondingly, the power spectrum for the smoothed velocity  $\mathbf{u}$  has two regimes, with a transition from  $k^{-5/3}$  for  $k\alpha < 1$  to  $k^{-3}$  for  $k\alpha > 1$ . Thus, the KH-theorem for the  $LANS-\alpha$  model derived in [26] is consistent with the spectral scaling results found for it in [23] by dimensional arguments. We shall apply similar reasoning to the  $LAMHD-\alpha$  model in two dimensions.

## Differences from MHD turbulence theory for $r < \alpha$

The second term in the “ $-2/d(d+2)$  Law” in equation (49) (the  $\alpha^2 \mathcal{S}$  term on the right side) is reminiscent of the quantity that appears in the corresponding “ $-2$  Law” for enstrophy cascade in 2D turbulence. The latter expression contains two powers of enstrophy and one power of velocity. For example, see the Appendix B of [29], where this identity for 2D turbulence is derived in detail.

Likewise, the  $\alpha^2 \mathcal{S}$  term in (49) for  $LAMHD-\alpha$  in 2D contains two powers of gradients  $\nabla \mathbf{z}_s$  and one power of  $\mathbf{z}_s$  without gradient. Consequently, this should be the dominant term (compared to the first  $\mathcal{T}$ -term) for small separations, when  $r < \alpha$ . If in addition the  $LAMHD-\alpha$  flow is *self-similar*, the dominance of the  $\alpha^2 \mathcal{S}$  term in (49) when  $r < \alpha$  implies a scaling relation for the second-order structure functions. Following [18] as amplified by [28], let the longitudinal difference  $\delta \mathbf{z}(\mathbf{x}, r)$  satisfy the scaling relation  $\delta \mathbf{z}(\mathbf{x}, \lambda r) = \lambda^h \delta \mathbf{z}(\mathbf{x}, r)$  for all  $\mathbf{x}$  and for increments  $r$  and  $\lambda r$  small compared to  $\alpha$ . By dimensional analysis,  $[\mathcal{S}(\lambda r)] = [(\delta \mathbf{z})^3 / r^3] = [\mathcal{S}(r)]$ . Consequently,  $3h - 3 = 0$  and  $h = 1$  for small scales  $r < \alpha$  in a self-similar  $LAMHD-\alpha$  flow. This means the *second-order* structure functions follow  $r^2$  scaling for  $r < \alpha$  in such a flow. This  $r^2$  scaling implies a  $k^{-3}$  law for the spectral density of smoothed kinetic and magnetic energy in that range for the 2D  $LAMHD-\alpha$  model. Thus, one finds a self-similar  $k^{-3}$  “enstrophy-like” cascade, in agreement with similar considerations of [23] for the kinetic energy



spectral density in the 3D LANS- $\alpha$  model.

**Implications of the  $k^{-5/3} \rightarrow k^{-3}$  spectral scaling transition for the  $LAMHD-\alpha$  dissipation anomaly.** The second term in the “ $-2/d(d+2)$  Law” in equation (49) modifies Kolmogorov’s four-fifths law at small separations ( $r < \alpha$ ), provided one may assume constancy of total  $LAMHD-\alpha$  energy dissipation as  $\nu \rightarrow 0$ . This is the “energy dissipation anomaly” for the  $LAMHD-\alpha$  model. A technical argument using embedding theorems for Besov spaces first introduced in [30] implies that constancy of total energy dissipation may hold as  $\nu \rightarrow 0$  for a turbulent fluid in two dimensions, provided its  $L^2$  power spectrum is not steeper than  $k^{-4}$ . The  $k^{-3}$  spectrum for  $k\alpha > 1$  is not too steep; so the roll-off  $k^{-5/3} \rightarrow k^{-3}$  in the  $LAMHD-\alpha$  power spectrum is consistent with the necessary condition for possessing such an energy dissipation anomaly. Hence, the  $k^{-3}$  behavior in the  $L^2$  power spectrum of the  $LAMHD-\alpha$  model for  $k\alpha > 1$  and the corresponding modification for separations  $r < \alpha$  of Kolmogorov’s four-fifths law derived in [26] are both consistent with the assumption of constant dissipation of *total* kinetic energy as the Reynolds number tends to infinity.

**Implications of the spectral scaling transition for IK scaling instead of Kolmogorov scaling.** While in hydrodynamic turbulence the spectral transfer is believed to be a local process, in MHD turbulence Iroshnikov and Kraichnan proposed that the spectral transfer is governed by nonlocal Alfvén wave interactions (see [31] for a study of non-locality of transfer in MHD). If a large scale magnetic field is present, then this field acts as a guide field to the fluctuations, turning them into Alfvén waves. Kraichnan proposed that Alfvénic propagation limits the nonlinear interaction responsible for the transfer of energy to smaller eddies in the absence of magnetic fields. As a result, the IK spectrum is shallower than K41. In  $LAMHD-\alpha$ , the  $k^{-3}$  spectrum at scales smaller than  $\alpha$  turns into a shallower  $k^{-5/2}$  when the IK hypotheses are used. Note that the weakening of local interactions due to Alfvén waves holds in  $LAMHD-\alpha$  at the smoothed scales, and the energy dissipation anomaly should also be captured. This is also in agreement with equations (25) and (27), which show that Alfvén waves are also exact nonlinear solutions of the  $LAMHD-\alpha$  equations.

## 6 Numerical results for intermittency and scaling anomaly

In this section, we compare intermittency in *LAMHD*– $\alpha$  to that of direct numerical simulations (DNS) of the MHD equations, regarded as true at a given Reynolds number. Intermittency is associated both with the presence of strong localized structures and with the existence of strong non-Gaussian wings in the probability distribution functions. We have previously investigated the latter in [11] and we concentrate here on the strong localized structures giving rise to deviations from universality, as can be studied by examining high order statistical moments, such as the structure functions.

We define the longitudinal structure function of a field  $\mathbf{f}$  as  $\mathfrak{S}_p^f(l) \equiv \langle |\delta f_L|^p \rangle$  where  $\delta f_L = (\mathbf{f}(\mathbf{x} + \mathbf{l}) - \mathbf{f}(\mathbf{x})) \cdot \mathbf{l}/l$  is the longitudinal increment of  $\mathbf{f}$ . In the inertial range between the large energy-containing scales and the small dissipative scales, the structure functions are assumed to vary in a self-similar manner,  $\mathfrak{S}_p^f(l) \sim l^{\zeta_p^f}$ . As previously mentioned, in isotropic and homogeneous turbulence the structure functions can be related to the correlation functions discussed in Section 4. K41 phenomenology predicts  $\zeta_p^v = p/3$ , while IK gives  $\zeta_p^\pm = p/4$ . The anomalous departure of the exponents  $\zeta_p$  from these linear scaling laws is a measure of intermittency-induced deviations from universality.

To numerically solve the MHD and *LAMHD*– $\alpha$  equations we will use a parallel pseudospectral code as described in [11]. In two dimensions, the velocity and magnetic field are expressed as the curl of a scalar stream function  $\Psi$  and a one component vector potential  $A_z$ , respectively:

$$\mathbf{u} = \nabla \times (\Psi \hat{\mathbf{z}}), \quad \mathbf{u}_s = \nabla \times (\Psi_s \hat{\mathbf{z}}) \quad (50)$$

$$\mathbf{B} = \nabla \times (A_z \hat{\mathbf{z}}), \quad \mathbf{B}_s = \nabla \times (A_{s_z} \hat{\mathbf{z}}) \quad (51)$$

where  $\Psi = (1 - \alpha^2 \nabla^2) \Psi_s$ , and  $A_z = (1 - \alpha_M^2 \nabla^2) A_{s_z}$ . In terms of these quantities, the 2D MHD equations may be expressed as

$$\partial_t \nabla^2 \Psi = [\Psi, \nabla^2 \Psi] - [A_z, \nabla^2 A_z] + \nu \nabla^2 \nabla^2 \Psi \quad (52)$$

$$\partial_t A_z = [\Psi, A_z] + \eta \nabla^2 A_z, \quad (53)$$

where

$$[F, G] = \partial_x F \partial_y G - \partial_x G \partial_y F \quad (54)$$

is the standard Poisson bracket. The *LAMHD*– $\alpha$  equations (1-3) modify this two dimensional structure by introducing smoothed variables as

$$\partial_t \nabla^2 \Psi = [\Psi_s, \nabla^2 \Psi] - [A_{s_z}, \nabla^2 A_z] + \nu \nabla^2 \nabla^2 \Psi \quad (55)$$

$$\partial_t A_{s_z} = [\Psi_s, A_{s_z}] + \eta \nabla^2 A_z. \quad (56)$$

In the following subsections we test the *LAMHD*– $\alpha$  model against MHD results (for which  $\alpha = \alpha_M = 0$ ) for freely decaying turbulence with the same initial conditions, dissipation and time-stepping, and also for forced turbulence where we have averaged statistics over 189 turnover times taken from 9 experiments with distinct seeds for the random forcing, resulting in a data set of  $\sim 2 \cdot 10^8$  points.

## 6.1 Forced simulations

In this subsection we consider forced turbulence with  $\eta = \nu = 1.6 \times 10^{-4}$ . Four sets of simulations were carried out, one set of MHD fully-resolved simulations with  $1024^2$  grid points, and three sets of *LAMHD*– $\alpha$  simulations, with  $512^2$  grid points and  $\alpha = \alpha_M = 6/512$ , with  $256^2$  grid points and  $\alpha = \alpha_M = 6/256$ , and with  $256^2$  grid points and  $\alpha = \alpha_M = 6/128$ . Note that the  $256^2$  *LAMHD*– $\alpha$  simulation with  $\alpha = \alpha_M = 6/128$  could be carried out with a  $128^2$  spatial resolution (see e.g. criteria for the selection of the value of  $\alpha$  and the linear resolution in [11]). The reason to keep the resolution fixed at  $256^2$  is to preserve the amount of spatial statistics, crucial to measure high order exponents as will be shown later.

Both the momentum and the vector potential equations were forced. The expressions of the external forces were loaded in the Fourier ring between  $k = 1$  and  $k = 2$ , and the phases were changed randomly with a correlation time  $\Delta t = 5 \times 10^{-2}$ . Averaged over space, the amplitudes of the external forces were held constant to  $F_M = 0.2$  in the vector potential equation, and  $F_K = 0.45$  in the momentum equation. The systems were evolved in time until reaching a turbulent steady state, and then the simulations were extended for 21 turnover times. Over this time span, 21 snapshots of the fields from each run were used to compute the longitudinal increments. As

previously mentioned, each set of simulations (DNS, and *LAMHD*– $\alpha$  with different spatial resolutions) comprises nine runs with the same viscosity and diffusivity but different series of random phases in the external forcing, to have enough statistics to determine the scaling exponents up to eighth order with small error bars. The total number of points was  $\sim 2 \cdot 10^8$  for the DNS and  $\sim 1.2 \cdot 10^7$  points for the  $256^2$  *LAMHD*– $\alpha$  simulations.

During these intervals, the integral Reynolds number based on the *r.m.s.* velocity fluctuates around 2200. The normalized correlation coefficient between the velocity and the magnetic field is 20% with a standard deviation of 16% within the set of nine runs, and its unsigned counterpart  $2\langle|\mathbf{u} \cdot \mathbf{B}|\rangle/\langle|\mathbf{u}|^2 + |\mathbf{B}|^2\rangle$ , is  $\sim 29\% \pm 12\%$ . The ratio of the integral scale to the Taylor scale computed on the *r.m.s.* fields fluctuates around 10 for all the simulations. The ratio of magnetic to kinetic energies is  $\sim 2$  for all runs. Finally, the Kolmogorov dissipation wavenumbers  $k_\nu = (\langle\omega^2\rangle/\nu^2)^{1/4}$  and  $k_\eta = (\langle j^2\rangle/\eta^2)^{1/4}$  fluctuate around 330, values substantially larger than the largest resolved wavenumbers  $k_\alpha \sim 1/\alpha$  in all *LAMHD*– $\alpha$  simulations, by virtue of the model.

Average omni-directional spectra for magnetic and kinetic energies over these 189 turnover times are shown in Figure 1. All spectra display an inertial range, and the *LAMHD*– $\alpha$  simulations are able to capture the spectral behavior up to  $k \approx 1/\alpha$ . For  $k > 1/\alpha$ , theoretical arguments suggest a  $k^{-3}$  spectrum for the alpha model. To observe this spectrum, however, large values of  $\alpha$  would be required. This is inconsistent with the use of the alpha model as a subgrid turbulent model, and lies beyond the interest of the present work.

K41 theory predicts

$$\mathfrak{S}_p^u(l) \sim l^{\zeta_p^u}, \quad (57)$$

which follows from the assumption that the statistical properties of the field are self-similar in the inertial range, which will be identified here as the scales for which the relation

$$\zeta_3^u = 1 \quad (58)$$

holds. The existence of scaling (57) has been extensively verified for the hydrodynamic case. Starting from the assumption of self-similarity in the inertial range, we can then postulate the validity of (57) at arbitrarily high order,  $p$ . From an experimental standpoint, the amount of data used in calculating  $\mathfrak{S}_p^u(l)$  determines the highest order for which we can observe a scaling in the inertial range. Above this order, the assumption of self-

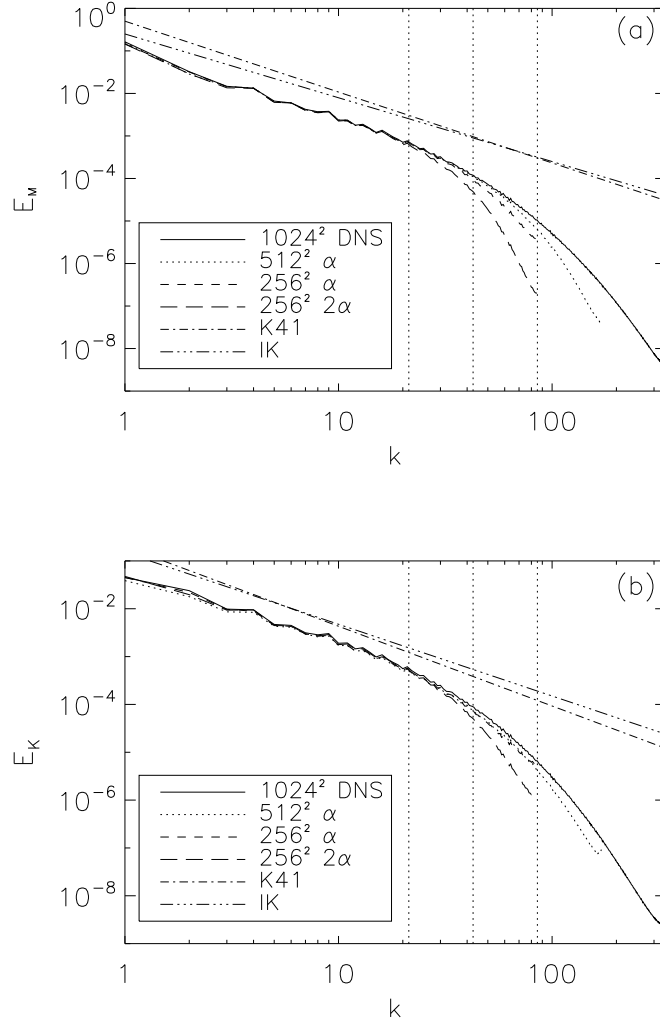


Figure 1: Spectra averaged over 189 turnover times.  $1024^2$  MHD is the solid line,  $512^2$  *LAMHD*– $\alpha$  is the dotted line,  $256^2$  *LAMHD*– $\alpha$  is the dashed line,  $256^2$  *LAMHD*– $\alpha$  with  $\alpha = \alpha_M = 6/128$  is the long-dashed line (hereafter indicated in figures as ‘ $256^2$   $2\alpha$ ’),  $k^{-5/3}$  (K41) is the dash-dotted line, and  $k^{-3/2}$  (IK) is the dash-triple-dotted line; the K41 and IK slopes are shown for reference. The vertical lines indicate the wavenumbers corresponding to the lengths  $\alpha$  for all *LAMHD*– $\alpha$  simulations. Panel (a) is magnetic energy,  $E_M$ , versus wavenumber  $k$ , and panel (b) is kinetic energy,  $E_K$  vs.  $k$ .

similarity allows us to fit a scaling law to our data in any event. But in the absence of sufficient statistics, such a fit can be poor and the error bars rather large (see, *e.g.*, Figure 4 and Figure 5 **(a)** to be discussed shortly).

The Extended Self-Similarity (ESS) hypothesis [32], proposes the scaling

$$\mathfrak{S}_p^u(l) \sim [\mathfrak{S}_3^u(l)]^{\xi_p^u}, \quad (59)$$

which is found to apply to a much wider scaling range than the inertial range. Here, the scaling range is determined by the observed scaling for low orders and a chief benefit is increased statistics to compute more accurate exponents at higher order. For the case of MHD, Ref. [22] proposes to replace  $\mathfrak{S}_3^u(l)$  with the third-order, mixed structure functions,  $L^\pm(l)$ . As in the ESS hypothesis, these scales  $L^\pm(l)$  may provide better independent variables (as opposed to length  $l$ ) against which to determine the scaling exponents for MHD. From the KH theorem for an incompressible, non-helical MHD flow, they find

$$\langle \delta z_L^\mp(\mathbf{1}) |\delta z^\pm(\mathbf{1})|^2 \rangle = -\frac{4}{d} \varepsilon^\pm l, \quad (60)$$

where  $|\delta z^\pm|^2 = (\delta z_L^\pm)^2 + (\delta z_T^\pm)^2$ ,  $\delta z_T^\pm$  are the transverse increments,  $d$  is the space dimension,  $\varepsilon^+$  and  $\varepsilon^-$  are the energy dissipation rates for  $\frac{1}{2}(z^+)^2$  and  $\frac{1}{2}(z^-)^2$  respectively, and angle brackets indicate as usual spatial averages [22].

These results for the third-order structure functions are exact and can be used to compute more accurate anomalous scaling exponents of structure functions of higher order. Due to cancellation problems (linked with having limited statistics), absolute values are often employed; we also find linear scaling in this case, *viz.*:

$$L^\pm(l) \equiv \langle |\delta z_L^\mp| |\delta z^\pm|^2 \rangle \propto l. \quad (61)$$

As follows from the expressions given in Sec. 4 and the invariants found for both MHD and *LAMHD*– $\alpha$  [11, 14], when making comparisons between DNS and model runs, we substitute the  $H_\alpha^1$  norm,  $\langle \|u\|_\alpha^2 \rangle = \langle |\mathbf{u} \cdot \mathbf{u}_s| \rangle$  [15, 33], for the regular  $L^2$  norm,  $\langle |u|^2 \rangle = \langle |\mathbf{u} \cdot \mathbf{u}| \rangle$ , whenever we consider quantities for the *LAMHD*– $\alpha$  model. The Karman-Howarth theorem for *LAMHD*– $\alpha$  is essential to this study of intermittency in that it allows us to define the structure functions for *LAMHD*– $\alpha$ ; it also identifies the flux relation that scales linearly with  $l$  for application in MHD of the ESS hypothesis. Accordingly we determine the relative scaling exponents,  $\xi_p^f$ , by using Eq. (61) for

the third-order, mixed structure function,  $L^+(l) = \langle |\delta z_L^-| |\delta z^+|^2 \rangle$  for MHD and  $L_s^+(l) = \langle |\delta z_{s_L}^-| |\delta z^+|^2 \rangle$  for LAMHD- $\alpha$ ,

$$\mathfrak{S}_p^f(l) \sim [L_{(s)}^+(l)]^{\xi_p^f}. \quad (62)$$

Figure 2 shows the third-order mixed structure function  $L_{(s)}^+(l)/l$  as a function of  $l$ . We find, contrary to what is reported in [17], that the relation (61) has a identifiable range of validity, as can be seen in the figure by comparison with the solid straight line denoting the computed slope  $L^+(l) \sim l^{0.99}$ . This range of validity is identified as the inertial range,  $2\pi/20 \leq l \leq 2\pi/10$ , indicated by dashed vertical lines. The LAMHD- $\alpha$  runs display the same scaling as the MHD simulation, and departures are pronounced only for scales approaching and smaller than  $\alpha$  (for the  $256^2$  runs,  $\alpha \approx 0.15, 0.29$  and for the  $512^2$  run,  $\alpha \approx 0.07$  as indicated by dotted vertical lines). Note that the results have been scaled by the mean value of  $L_{(s)}^+(l)$ . As the average energies of the runs are disparate, this improves the ease of comparison. The same behavior is observed for  $L_{(s)}^-(l)$ .

The scaling of the third-order structure function  $\mathfrak{S}_3^+$  versus  $L_{(s)}^+$  for the Elsässer variable  $\mathbf{z}^+$  is shown in Figure 3 (a) as well as a compensated plot versus  $l$  in Figure 3 (b). We see very little contamination at scales larger than  $\alpha$ . This contrasts with hyperviscosity which is known to cause an enhanced bottleneck in Navier-Stokes turbulence, which corrupts the scaling of the larger scales for structure functions of order two and higher [39]. The MHD case has not been studied in this context, and the presence of an inverse cascade of magnetic helicity might also exacerbate the problem.

The LAMHD- $\alpha$  simulations show similar scaling to what is found in DNS of MHD. A solid line indicates the best fit to the DNS data,  $\xi_3^+ = 1.01 \pm 0.08$  using the ESS hypothesis (the ESS scaling range is indicated by dotted vertical lines); note that all errors presented and shown in the figures correspond to  $3\sigma$  where  $\sigma$  is the standard deviation. The much smaller inertial range is indicated by dashed vertical lines and arrows indicate lengths  $\alpha$ . This is the main benefit of using the ESS hypothesis. While in the  $1024^2$  simulation there is enough statistics to measure the scaling exponents  $\xi_p$  in the inertial range, when we use the LAMHD- $\alpha$  equations to reduce the computational cost, the amount of spatial statistics is drastically reduced (e.g. by a factor of 16 in the  $256^2$  runs). The ESS hypothesis allows us to extend the range where the  $\xi_p$  exponents are computed, giving a better

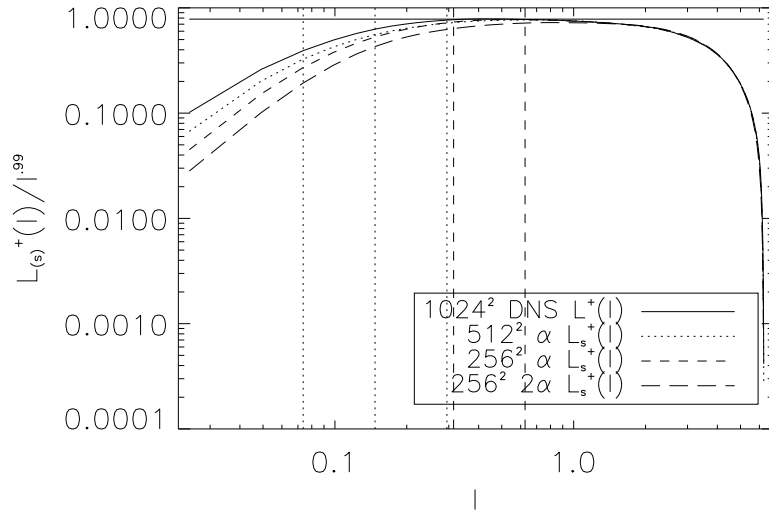


Figure 2: Third-order, mixed structure function,  $L_{(s)}^+(l)/l^{0.99}$ , versus  $l$ , for forced runs of turbulence averaged over 189 turnover times. Results are scaled by the mean value of  $L_{(s)}^+(l)$  for easier comparison. Labels are as in Fig. 1. The best fit to the MHD data,  $L^+ \sim l^{0.99}$ , is indicated by the solid straight line. The inertial range where this fit is made is indicated by dashed vertical lines and dotted vertical lines indicate the lengths  $\alpha$  for the  $512^2$  and  $256^2$  simulations.



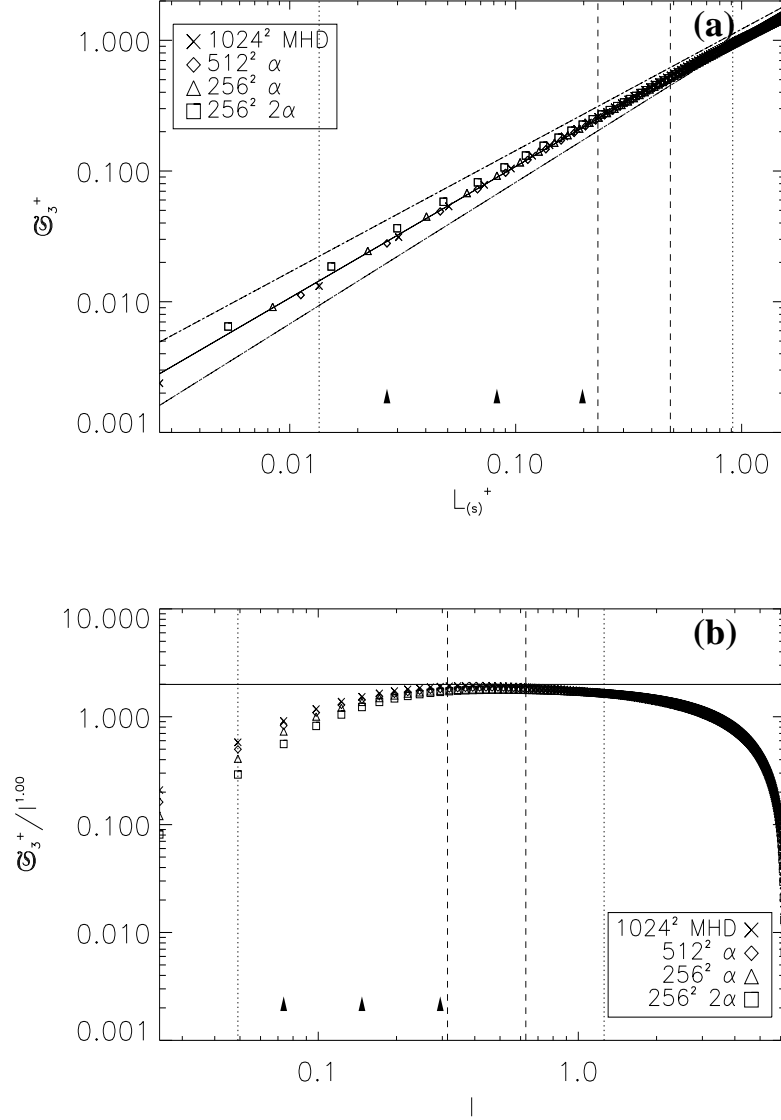


Figure 3: Third-order structure functions for  $\mathbf{z}^+$ : Panel (a)  $\mathfrak{S}_3^+$  versus  $L_{(s)}^+$  and panel (b)  $\mathfrak{S}_3^+/l^3$  versus  $l$ , computed over 189 turnover times. Labels are as in Fig. 1. The solid line corresponds to the best fit to the DNS data,  $\mathfrak{S}_3^+ = (L^+)^{1.01}$  (the dash-dotted lines represent the  $3\sigma$  error). The ESS hypothesis range where this fit is made is indicated by dotted vertical lines and dashed vertical lines indicate the inertial range. Arrows indicate the several lengths  $\alpha$  used in the simulations.

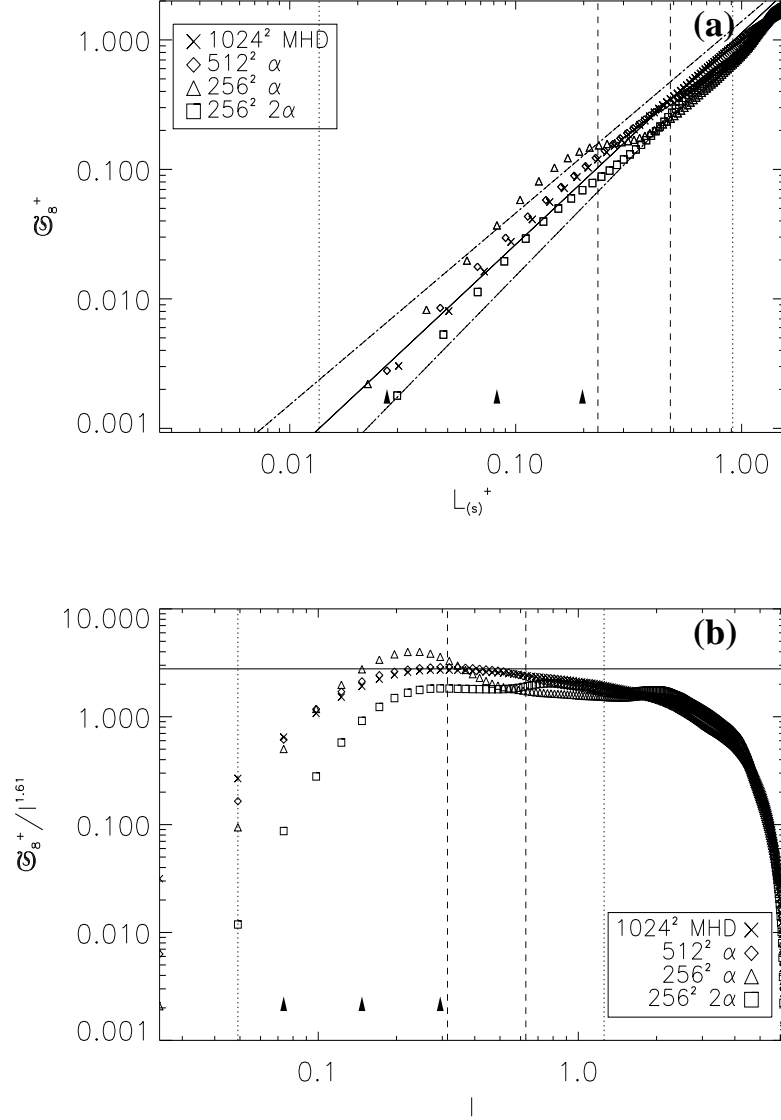


Figure 4: Eighth-order structure functions for  $\mathbf{z}^+$ : Panel (a)  $\mathfrak{S}_8^+$  versus  $L_{(s)}^+$  and panel (b)  $\mathfrak{S}_8^+ / l^{\zeta_8^+}$  versus  $l$ , computed over 189 turnover times. Labels are as in Fig. 3. The solid line corresponds to the best fit to the DNS data,  $\mathfrak{S}_8^+ = (L^+)^{1.63}$ . The ESS hypothesis range where this fit is made is indicated by dotted vertical lines and dashed vertical lines indicate the inertial range. Arrows indicate lengths  $\alpha$ .

estimation and smaller error bars. As an example, in Fig. 4 **(a)** we show the scaling of the eighth-order structure function  $\mathfrak{S}_8^+$  versus  $L_{(s)}^+$  as well as a compensated plot versus  $l$  in Figure 4 **(b)**. The ranges corresponding to the inertial range and ESS are also indicated. For the  $256^2$  runs, we cannot observe a scaling at this order. The error of a scaling computed from the assumption of self-similarity is excessively large (see Figure 5 **(a)**). From the ESS hypothesis a better estimation of the (postulated) scaling at order eight can be made (see Figure 5 **(b)**).

Figure 5 compares the scaling exponents,  $\xi_p^+$ , for the DNS runs and the three sets of *LAMHD*– $\alpha$  runs. Figure 5 **(a)** is for exponents computed only over the inertial range. Notice that the *LAMHD*– $\alpha$  runs capture the scaling for the low-order moments ( $p \leq 4$ ). For higher-order moments (beginning at  $p = 5$ ), the drop in the scaling exponents for the  $256^2$  results (with  $\alpha = \alpha_M = 6/256$ ) and the large error bars are indicative of insufficient statistics. The advantages of ESS are clearly seen by comparison with Figure 5 **(b)**, which shows the scaling exponents for all sets of runs employing the ESS hypothesis. In both figures, the She-L ev eque (SL) formula [35] modified for the MHD case [21] is shown as a reference,

$$\frac{\xi_p}{\xi_3} = \frac{p}{6} + 1 - \left(\frac{1}{2}\right)^{p/3}. \quad (63)$$

From these results, we conclude that *LAMHD*– $\alpha$  captures the intermittency of the DNS runs up to and including the eighth-order moment (to within the errors of our statistics). The size of the error bars make it difficult to draw further conclusions from the data.

The anomalous scaling results for the DNS runs are shown in Table 1. Though our goal here is to test *LAMHD*– $\alpha$  against DNS, we remark briefly on the correspondence between our scaling exponents and other studies. In opposition to the findings of [36], we find  $\xi_3^\pm \sim 1$  but  $\xi_4^\pm > 1$ . We note, however, that the forcing in [36] was tailored to maintain at a constant level all Fourier modes with  $k = 1$  while our forcing is random with a constant amplitude between  $k = 1$  and  $k = 2$ . As can be seen from Table 1, our results for  $\xi_p^+$  are in good agreement with [17], for decaying turbulence, and with [37], for forced turbulence. As [17] suggests, the scaling exponents, as inertial range properties, may depend on the character of the driving due to non-local processes in the cascade dynamics connected with the Alfv en effect (see also [31]); and as Ref. [36] points out, such an analysis can be sensitive

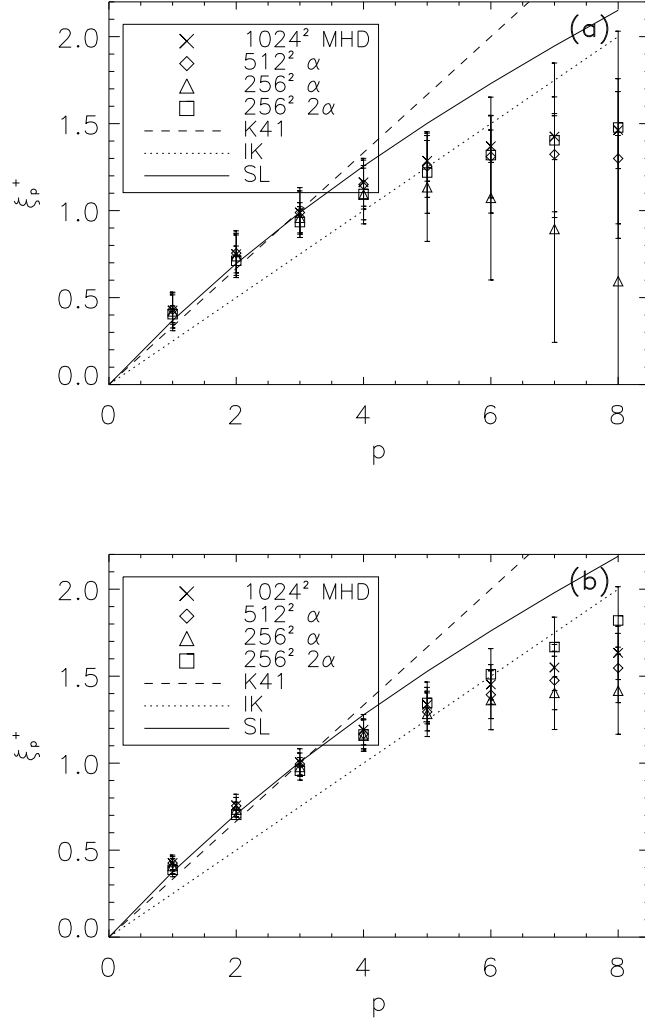


Figure 5: Structure function scaling exponent:  $\xi_p^+$  versus  $p$ , computed over 189 turnover times.  $1024^2$  MHD are the pluses,  $512^2$  *LAMHD*– $\alpha$  are the diamonds,  $256^2$  *LAMHD*– $\alpha$  ( $\alpha = 6/256$ ) are triangles, and  $256^2$  *LAMHD*– $\alpha$  ( $\alpha = 6/128$ ) are the squares. The dashed line indicates K41 scaling, dotted line indicates IK scaling, and the solid line is the prediction using the modified She-L ev eque formula (see text). Panel (a) is computed over the inertial range. Panel (b) is computed utilizing the ESS hypothesis.

Table 1: Relative scaling exponents (together with  $3\sigma$  errors in computing the slope in parenthesis) computed from the 9 MHD runs over the inertial range,  $\xi$ , and utilizing the ESS hypothesis,  $\xi_{ESS}$ .

$p$	$\xi^+$	$\xi_{ESS}^+$	$\xi_{ESS}^-$	$\xi_{ESS}^u$	$\xi_{ESS}^B$
1	.43(10)	.43(05)	.42(04)	.37(06)	.43(04)
2	.75(13)	.76(06)	.76(04)	.67(08)	.76(04)
3	.99(14)	1.01(08)	1.01(03)	.92(08)	1.01(04)
4	1.16(14)	1.19(09)	1.20(04)	1.10(08)	1.16(02)
5	1.29(11)	1.34(10)	1.34(07)	1.25(08)	1.27(04)
6	1.37(09)	1.45(11)	1.45(09)	1.36(05)	1.33(06)
7	1.43(13)	1.55(13)	1.53(12)	1.44(11)	1.38(07)
8	1.46(22)	1.63(15)	1.60(14)	1.50(13)	1.43(08)

to several parameters such as the ratio of kinetic to magnetic energy or the amount of correlation between the velocity and the magnetic fields.

Figure 6 shows the scaling exponents for the velocity and magnetic fields, as well as for the other Elsässer variable  $\mathbf{z}^-$ . The anomalous scaling is again matched by *LAMHD*– $\alpha$  up to and including eighth-order. The results from the MHD and *LAMHD*– $\alpha$  simulations are also in good agreement with Ref. [37]. Note that the magnetic field is more intermittent than the velocity field (in the sense that the scaling exponents deviate more from a straight line), as previously found in numerical simulations [36]; it may be related to the fact that in MHD, nonlinear interactions are more non-local (in Fourier space) than for fluids [31]. This well known feature of MHD turbulence is also properly captured by the *LAMHD*– $\alpha$  equations. The average (over all fields) of the  $3\sigma$  errors of the eighth order scaling exponent is 0.13 for the DNS on a  $1024^2$  grid; it is 0.15 and 0.16 for *LAMHD*– $\alpha$  on a  $512^2$  and  $256^2$  grid, respectively. To further test the convergence of our statistics, we reduced the amount of data used to compute the scaling exponents for the  $512^2$  runs by a factor of 4 (which gives the same amount of statistics than the  $256^3$  *LAMHD* runs) and determined an average  $3\sigma$  error of 0.17. While these results confirm our convergence as the amount of statistics is increased, they also highlight the rather low decrease in error with increased computational effort. Accordingly, the computational burden for more accurate

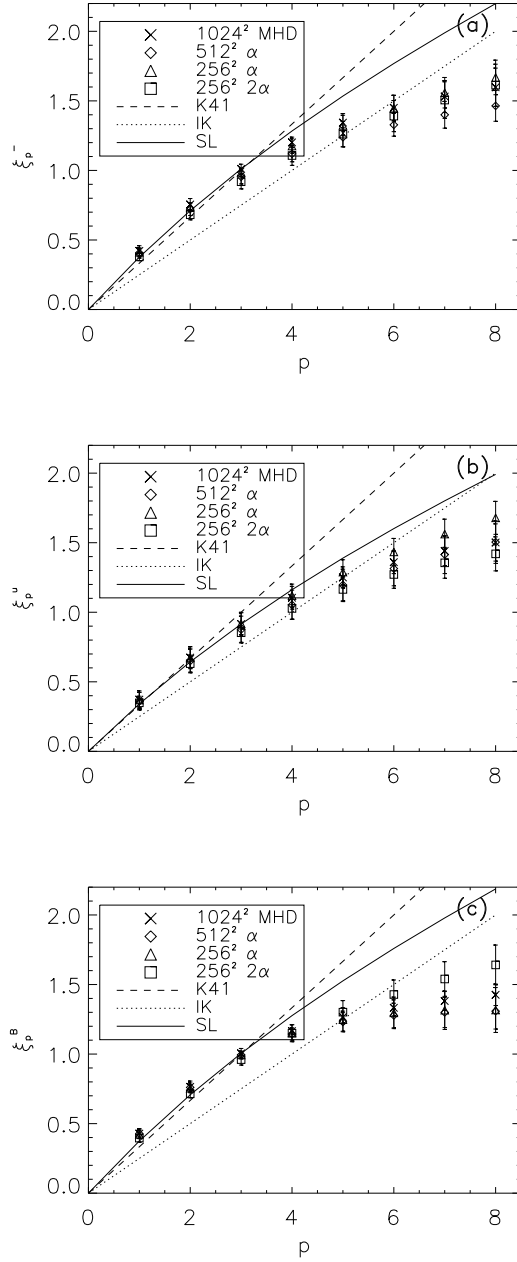


Figure 6: Structure-function scaling exponent  $\xi_p^+$  versus  $p$  for  $\mathbf{z}^-$  (panel (a)),  $\mathbf{u}$  (panel (b)), and  $\mathbf{B}$  (panel (c)). Labels are as in Figure 5.

determination of high-order statistics prohibits further analysis of the data.

## 6.2 Decaying simulations

In this subsection we briefly discuss simulations of free decaying turbulence using both the MHD and the *LAMHD*– $\alpha$  equations. The results are similar to the ones presented in the previous subsection for forced turbulence. However, since no turbulent steady state can be defined in freely decaying runs, the amount of statistics is reduced as only a few snapshots of the velocity and magnetic field during the peak of mechanic and magnetic dissipation can be used to compute structure functions. To partially overcome this problem, we will discuss simulations with higher spatial resolution than the ones presented in the forced case.

A fully resolved  $2048^2$  MHD run was made using  $\nu = \eta = 10^{-4}$ , as well as a  $1024^2$  *LAMHD*– $\alpha$  run with  $\alpha = \alpha_M = 6/1024$  and a  $512^2$  *LAMHD*– $\alpha$  run with  $\alpha = \alpha_M = 6/512$ . The initial velocity and magnetic fields were loaded with random phases into the rings from  $k = 1$  to  $k = 3$  in Fourier space. The initial *r.m.s.* values of  $\mathbf{u}$  and  $\mathbf{B}$  are equal to unity. No external forces are applied and the system decays freely as a result of the dissipation. Under these conditions, the *LAMHD*– $\alpha$  equations have been shown to reproduce the time evolution of the magnetic and kinetic energy, as well as the evolution of the spectra and other statistical quantities [11].

The magnetic and kinetic energy spectra between  $t = 3$  and  $t = 6$  in units of the eddy turnover time (the time for which a quasi-steady state is observed) display an inertial range with an extent of approximately one decade in Fourier space, from  $k \approx 3$  up to  $k \approx 30$ . As a result, one snapshot of the fields in this range in time was used to compute the longitudinal structure functions. The Kolmogorov kinetic and magnetic dissipation wavenumbers  $k_\nu$  and  $k_\eta$  peaked at a value of 470, larger than the filtering wavenumber  $k_\alpha \sim 1/\alpha$  in all the *LAMHD*– $\alpha$  simulations. We note that for large wavelength component behavior up to  $k \sim k_\alpha$ , both *LAMHD*– $\alpha$  simulations accurately reproduced the omni-directional spectra for the magnetic and kinetic energies as was shown previously for the forced runs.

Both *LAMHD*– $\alpha$  runs preserve the scaling of the longitudinal structure function exponents observed in the MHD simulation. As an example, Fig. 7 shows the  $\xi_p$  exponents for the  $\mathbf{z}^+$  Elsässer variable for the MHD and *LAMHD*– $\alpha$  simulations using the ESS hypothesis. Note that the  $\xi_p$  exponents of the three simulations lie within the error bars, and the three simula-

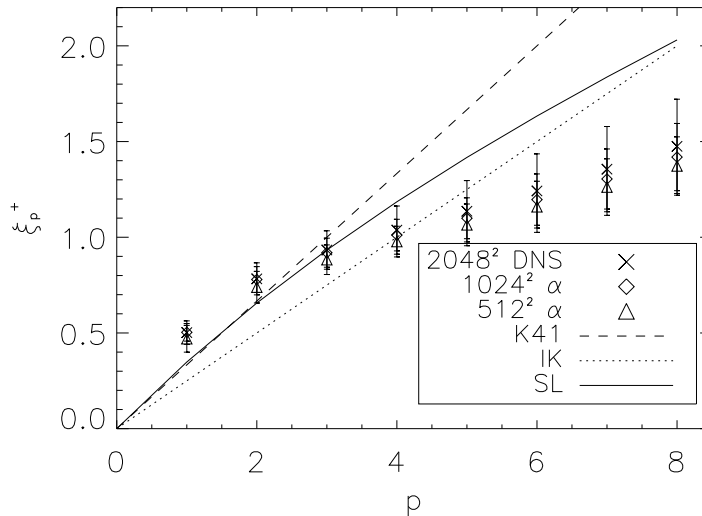


Figure 7: Scaling exponent  $\xi_p^+$  as a function of the order  $p$ , for the  $\mathbf{z}^+$  Elsässer variable in simulations of freely-decaying turbulence. The MHD simulation, the  $1024^2$  *LAMHD*– $\alpha$  run, and the  $512^2$  *LAMHD*– $\alpha$  run are denoted by crosses, diamonds, and triangles respectively. The K41 scaling is the dashed line, the IK prediction is the dotted line, and the solid line corresponds to eq. (63).

tions show departures from the self-similar K41 or IK scaling. For values of  $p$  larger than 6, effects associated with the limited amount of spatial statistics can be observed in all the runs.

## 7 Discussion and outlook

Sufficient resolution for studying directly high Reynolds number flows as encountered in geophysics and astrophysics is today well beyond technological limits. Closures such as the Lagrangian-averaged alpha-model can reduce the computational burden by reducing the resolution requirements. However, to be used as a model of hydrodynamic or magnetohydrodynamic turbulence, or for applications in astrophysics and geophysics, detailed knowledge of the



ability of the  $LANS-\alpha$  or  $LAMHD-\alpha$  equations to capture key features of turbulent flows is required.

The  $LANS-\alpha$  and  $LAMHD-\alpha$  equations have been tested against direct numerical simulations in a variety of problems (see *e.g.* [38] for neutral fluid studies and [11, 12, 13] for studies in conducting fluids). Most of these works compared the time evolution of ideal invariants for forced and free decaying turbulence, as well as the evolution of energy spectra. Also, some statistical comparisons were performed (*e.g.* studying the behavior of probability density functions). In this work, we apply a more stringent test to these models. Intermittency is a well known feature of turbulent flows, associated with the existence of strong events localized both in space and time. Intermittency can trigger large scale events, affect the transport coefficients, or give rise to corrections in the turbulent scaling. As a result, whether a model can capture the statistics of intermittent events is of utmost importance to model astrophysical or geophysical flows. The study of intermittency also requires computation of high order statistics, thereby extending previous comparisons between DNS and  $\alpha$ -models.

An extension of the Kármán-Howarth theorem (KH- $\alpha$ ) was proven for the  $LANS-\alpha$  equations in Ref. [26]. As a corollary of this theorem, Kolmogorov four-fifths law and Kolmogorov's energy spectrum can be derived for the  $LANS-\alpha$  equations at scales larger than  $\alpha$ . In this work, we extended the KH- $\alpha$  theorem to the  $LAMHD-\alpha$  case, proving as a result that for scales larger than  $\alpha$  the  $LAMHD-\alpha$  equations satisfy the scaling laws previously known for MHD turbulence [22, 25]. This is an important result, since MHD turbulence involves two coupled fields (the velocity and magnetic fields) and can display different power laws in the inertial range according to the regime of interest. While LES often impose a particular regime and a power law [7, 8, 9, 10], the  $LAMHD-\alpha$  equations are shown to satisfy the general scalings satisfied by the MHD equations without any hypothesis about the scaling followed in the inertial range.

The extension of the KH- $\alpha$  theorem to the  $LAMHD-\alpha$  case also allows us to define correlation and structure functions in the  $\alpha$ -model. With these functions, the analysis of anomalous scaling and intermittency can be performed. Numerical simulations were carried out both for freely decaying and for forced two dimensional MHD turbulence, solving directly the MHD equations, and employing the  $LAMHD-\alpha$  equations at 1/2 and 1/4 resolution (a case equivalent to 1/8 of the DNS resolution was also considered for forced turbulence). In the forced runs, we have averaged statistics over 189 turn-

over times (and up to  $\sim 2 \cdot 10^8$  points) to test if the *LAMHD*– $\alpha$  equations reproduces intermittent turbulent behavior. The scaling of the third-order structure function was tested and linear scaling with length (down to length  $\alpha$ ) was observed, in good agreement with corollaries of the extended KH- $\alpha$  theorem and exact laws in MHD turbulence [22]. The *LAMHD*– $\alpha$  equations also capture high-order statistics (up to and including order 8) and the anomalous scaling of the longitudinal structure function exponents, with a net gain in speed close to a factor of 16. For lower order structure functions, very little contamination of the scaling could be detected at scales larger than  $\alpha$ . On the other hand, for the highest computed order, fluctuations in the scaling are observed for the runs with the smallest resolution. Note that we would not expect any scaling to be preserved for  $\alpha$  so large that no inertial range remains.

Turbulence closures are never unique. The present case may owe its success not to its particular form, but rather to its general properties that it (1) preserves physical avenues of nonlinear energy exchange and (2) allows correct vortex stretching. These two properties derive from its origin via a Lagrangian-averaged Hamilton's principle. The derivation also identifies the appropriate dissipation for proper energy decay, which involves an enhanced resistivity, but not an enhanced viscosity. Together, the Navier-Stokes viscosity and the enhanced resistivity produce regularization (*e.g.*, existence and uniqueness of strong solutions and their global attractor of finite Hausdorff dimension, to be discussed elsewhere). In turn, these choices of viscosity and resistivity allow the intermittency found here, which might have otherwise been suppressed.

Relying on the fact that, contrary to fluids, two dimensional MHD turbulence displays a direct cascade of energy and intermittency, we could show that the *LAMHD*– $\alpha$  equations reproduce intermittency features of turbulent flows and thus we postulate that these results will carry over to the three-dimensional case and thus these results could be also of relevance to the modeling of neutral fluids. Future challenges will include implementation of the *LAMHD*– $\alpha$  model in domains with boundaries and the study of intermittency for magnetic Prandtl numbers besides unity. The choices of boundary conditions may be expected to strongly influence the solution behavior. Of course, this matter is beyond the scope of the present article.

## Acknowledgements

Computer time was provided by NCAR. The NSF grant CMG-0327888 at NCAR supported this work and is gratefully acknowledged. DDH is grateful for partial support by the US Department of Energy, under contract W-7405-ENG-36 for Los Alamos National Laboratory, and Office of Science ASCAR/AMS/MICS.

## References

- [1] P. Hoyng, M. A. J. H. Ossendrijver, and D. Schmitt, “The geodynamo as a bistable oscillator,” *Geophys. Astrophys. Fluid Dyn.* **94**, 263 (2001); P. Hoyng, D. Schmitt, and M. A. J. H. Ossendrijver, “A theoretical analysis of the observed variability of the geomagnetic dipole field,” *Phys. of Earth and Plan. Int.* **130**, 143-157 (2002).
- [2] P. Hoyng, “Helicity fluctuations in mean field theory: an explanation for the variability of the solar cycle?,” *Astron. Astrophys.* **272**, 321 (1993); A. J. H. Ossendrijver, and P. Hoyng, “Stochastic and nonlinear fluctuations in a mean field dynamo,” *Astron. Astrophys.* **313**, 959-970 (1996).
- [3] P. Charbonneau, “Multiperiodicity, Chaos, and Intermittency in a Reduced Model of the Solar Cycle,” *Sol. Phys.* **199**, 385-404 (2001); P. D. Mininni, D. O. Gómez, and G. B. Mindlin, “Biorthogonal Decomposition Techniques Unveil the Nature of the Irregularities Observed in the Solar Cycle,” *Phys. Rev. Lett.* **89**, 061101 (2002); P. Charbonneau, G. Blais-Laurier, and C. St-Jean, “Intermittency and Phase Persistence in a Babcock-Leighton Model of the Solar Cycle,” *Astrophys. J.* **616**, L183-L186 (2004); P. D. Mininni, and D. O. Gómez, “A new technique for comparing solar dynamo models and observations,” *Astron. Astrophys.* **426**, 1065-1073 (2004).
- [4] J. R. Kulkarni, L. K. Sadani, and B. S. Murthy, “Wavelet Analysis of Intermittent Turbulent Transport in the Atmospheric Surface Layer over a Monsoon Trough Region,” *Boundary-Layer Meteorology* **90**, 217 - 239 (1999).

- [5] S. Cerutti and C. Meneveau, “Intermittency and relative scaling of subgrid-scale energy dissipation in isotropic turbulence,” *Phys. Fluids* **10**, 928-937 (1998).
- [6] C. Meneveau and J. Katz, “Scale-Invariance and turbulence models for Large-Eddy Simulation,” *Annu. Rev. Fluid Mech.* **32**, 1-32 (2000).
- [7] A. Pouquet, U. Frisch, and J. Léorat, “Strong MHD helical turbulence and nonlinear dynamo effect,” *J. Fluid Mech.* **77**, 321-354 (1976); A. Yoshizawa, “Subgrid modeling for magnetohydrodynamic turbulent shear flows,” *Phys. Fluids* **30**, 1089-1095 (1987).
- [8] D. W. Longcope and R. N. Sudan, “Renormalization group analysis of reduced magnetohydrodynamics with application to subgrid modeling,” *Phys. Fluids B* **3**, 1945-1962 (1991); O. Agullo, W.-C. Müller, B. Knaepen, and D. Carati, “Large eddy simulation of decaying magnetohydrodynamic turbulence with dynamic subgrid-modeling,” *Phys. Plasmas* **8**, 3502-3505 (2001); W.-C. Müller and D. Carati, “Dynamic gradient-diffusion subgrid models for incompressible magnetohydrodynamic turbulence,” *Phys. Plasmas* **9**, 824-834 (2002).
- [9] M. Theobald, P. A. Fox, and S. Sofia, “A subgrid-scale resistivity for magnetohydrodynamics,” *Phys. Plasmas* **1**, 3016-3032 (1994); Y. Zhou, O. Schilling, and S. Ghosh, “Subgrid scale and backscatter model for magnetohydrodynamic turbulence based on closure theory: Theoretical formulation,” *Phys. Rev. E* **66**, 026309 (2002).
- [10] B. Knaepen and P. Moin, “Large-eddy simulation of conductive flows at low magnetic Reynolds number,” *Phys. Fluids* **16**, 1255-1261 (2004); Y. Ponty, H. Politano, and J.-F. Pinton, “Simulation of Induction at Low Magnetic Prandtl Number,” *Phys. Rev. Lett.* **92**, 144503 (2004).
- [11] P.D. Mininni, D.C. Montgomery, and A. Pouquet, “A numerical study of the alpha model for two-dimensional magnetohydrodynamic turbulent flows,” *Phys. Fluids* **17**, 035112 (2005).
- [12] P.D. Mininni, D.C. Montgomery, and A. Pouquet, “Numerical solutions of the three-dimensional magnetohydrodynamic alpha-model,” *Phys. Rev. E* **71**, 046304 (2005).

- [13] Y. Ponty, P.D. Mininni, D.C. Montgomery, J.-F. Pinton, H. Politano, and A. Pouquet, “Numerical study of dynamo action at low magnetic Prandtl numbers,” *Phys. Rev. Lett.* **94**, 164502 (2005).
- [14] D.D. Holm, “Fluctuation effects on 3D Lagrangian mean and Eulerian mean fluid motion,” *Physica D* **133**, 215-269 (1999); D.D. Holm, “Averaged Lagrangians and the mean dynamical effects of fluctuations in continuum mechanics,” *Physica D* **170**, 253-286 (2002); D.D. Holm, “Lagrangian averages, averaged Lagrangians, and the mean effects of fluctuations in fluid dynamics,” *Chaos* **12**, 518-530 (2002).
- [15] D.D. Holm, J.E. Marsden, and T.S. Ratiu, “The Euler–Poincaré equations and semidirect products with applications to continuum theories,” *Adv. Math.* **137**, 1-81 (1998).
- [16] D. Montgomery and A. Pouquet, “An alternative interpretation for the Holm ‘alpha model’,” *Phys. Fluids* **14**, 3365–3366 (2002).
- [17] D. Biskamp and E. Schwarz, “On two-dimensional magnetohydrodynamic turbulence,” *Phys. Plasmas* **8**, 3282-3292 (2001).
- [18] A.N. Kolmogorov, “The local structure of turbulence in incompressible viscous fluid for very large Reynolds number,” *Dok. Akad. Nauk SSSR* **30**, 9-13 (1941); “On degeneration (decay) of isotropic turbulence in an incompressible viscous liquid,” *Dok. Akad. Nauk SSSR* **31**, 538-540 (1941); “Dissipation of energy in locally isotropic turbulence,” *Dok. Akad. Nauk SSSR* **32**, 16-18 (1941).
- [19] P.S. Iroshnikov, “Turbulence of a conducting fluid in a strong magnetic field,” *Sov. Astron.* **7**, 566-571 (1963); R.H. Kraichnan, “Inertial-range spectrum of hydromagnetic turbulence,” *Phys. Fluids* **8**, 1385-1387 (1965).
- [20] S. Galtier, S.V. Nazarenko, A.C. Newell, A. Pouquet, “A weak turbulence theory for incompressible magnetohydrodynamics,” *J. Plasma Phys.* **63**, 447-488 (2000).
- [21] H. Politano and A. Pouquet, “Model of intermittency in magnetohydrodynamic turbulence,” *Phys. Rev. E* **52**, 636-641 (1995).

- [22] H. Politano and A. Pouquet, “von Kármán-Howarth equation for magnetohydrodynamics and its consequences on third-order longitudinal structure and correlation functions,” *Phys. Rev. E* **57**, 21-24 (1998); “Dynamical length scales for turbulent magnetized flows,” *Geophys. Res. Lett.* **25**, 273-276 (1998).
- [23] C. Foias, D.D. Holm, and E.S. Titi, “The Navier-Stokes-alpha model of fluid turbulence,” *Physica D* **152**, 505-519 (2001).
- [24] T. von Kármán and L. Howarth, “On the statistical theory of isotropic turbulence,” *Proc. Roy. Soc. London, Ser. A* **164**, 192-215 (1938).
- [25] S. Chandrasekhar, “The invariant theory of isotropic turbulence in magneto-hydrodynamics,” *Proc. Roy. Soc. London, Ser. A* **204**, 435-449 (1951).
- [26] D.D. Holm, “Kármán-Howarth theorem for the Lagrangian-averaged Navier-Stokes-alpha model of turbulence,” *J. Fluid Mech.* **467**, 205-214 (2002).
- [27] S. Chandrasekhar, “The theory of axisymmetric turbulence,” *Philos. Trans. R. Soc. London, Ser. A* **242**, 557-577 (1950).
- [28] U. Frisch, *Turbulence: the legacy of A.N. Kolmogorov* (Cambridge University Press, Cambridge, 1995).
- [29] G.L. Eyink, “Exact results on stationary turbulence in 2D: consequences of vorticity conservation,” *Physica D* **91**, 97-142 (1996).
- [30] P. Constantin, W. E, and E.S. Titi, “Onsager’s conjecture on the energy conservation for solutions of Euler’s,” *Commun. Math. Phys.* **165**, 207-209 (1994); G.L. Eyink, “Local 4/5-law and energy dissipation anomaly in turbulence,” *Nonlinearity* **16**, 137-145 (2003).
- [31] A. Alexakis, P.D. Mininni, and A. Pouquet, “Shell to shell energy transfer in MHD, Part I: steady state turbulence,” *Phys. Rev. E* **72**, 046301 (2005). P.D. Mininni, A. Alexakis, and A. Pouquet, “Shell to shell energy transfer in MHD, Part II: kinematic dynamo,” *Phys. Rev. E* **72**, 046302 (2005).

- [32] R. Benzi, S. Ciliberto, C. Baudet, G. Ruiz Chavarria, and R. Tripiccione, “Extended self-similarity in the dissipation range of fully developed turbulence,” *Europhysics Letters* **24**, 275-279 (1993); R. Benzi, S. Ciliberto, R. Tripiccione, C. Baudet, F. Massaioli, and S. Succi, “Extended self-similarity in turbulent flows,” *Phys. Rev. E* **48**, R29-R32 (1993); R. Benzi, L. Biferale, S. Ciliberto, M.V. Struglia, and R. Tripiccione, “Generalized scaling in fully developed turbulence,” *Physica D* **96**, 162-181 (1996).
- [33] D.D. Holm, J.E. Marsden, and T.S. Ratiu, “Euler-Poincaré Models of Ideal Fluids with Nonlinear Dispersion,” *Phys. Rev. Lett.* **80**, 4173-4176 (1998).
- [34] N. E. L. Haugen and A. Brandenburg, “Inertial range scaling in numerical turbulence with hyperviscosity,” *Phys. Rev. E* **70**, 026405 (2004).
- [35] Z.-S. She and E. Lévéque, “Universal scaling laws in fully developed turbulence,” *Phys. Rev. Lett.* **72**, 336-339 (1994).
- [36] H. Politano, A. Pouquet, and V. Carbone, “Determination of anomalous exponents of structure functions in two-dimensional magnetohydrodynamic turbulence,” *Europhysics Letters* **43**, 516-521 (1998).
- [37] T. Gomez, H. Politano, and A. Pouquet, “On the validity of a nonlocal approach for MHD turbulence,” *Phys. Fluids* **11**, 2298-2306 (1999).
- [38] S.Y. Chen, C. Foias, D.D. Holm, E.J. Olson, E.S. Titi, and S. Wynne, “A connection between the Camassa-Holm equations and turbulence in pipes and channels,” *Phys. Fluids* **11**, 2343-2353 (1999); S.Y. Chen, D.D. Holm, L.G. Margolin, and R. Zhang, “Direct numerical simulations of the Navier-Stokes alpha model,” *Physica D* **133**, 66-83 (1999).
- [39] N. E. L. Haugen and A. Brandenburg, “Intertial range scaling in numerical turbulence with hyperviscosity,” *Phys. Rev. E* **70**, 026405 (2004).